Judith Maja Biedermann, BSc

Elektrochemische Untersuchungen von Organometall-verbindungen mit Elementen der Gruppe 14

Electrochemical investigations on organometallic compounds containing group 14 elements

MASTERARBEIT

zur Erlangung des akademischen Grades

Diplom-Ingenieurin

Masterstudium Technische Chemie

eingereicht and der

Technischen Universität Graz

Betreuer

Univ.-Prof. Dipl.-Chem. Dr. rer. nat. Frank Uhlig
Institut für Anorganische Chemie

Dr. Ilie Hanzu
Institut für Chemische Technologie von Materialien

Graz, November 2014

Deutsche Fassung:

Beschluss der Curricula-Kommission für Bachelor-, Master- und Diplomstudien vom 10.11.2008

Genehmigung des Senates am 1.12.2008

EIDESSTATTLICHE ERKLÄRUNG

Ich erkläre an Eides statt, dass ich die vorliegende Arbeit selbstständig verfasst, andere als die angegebenen Quellen/Hilfsmittel nicht benutzt, und die den benutzten Quellen wörtlich und inhaltlich entnommene Stellen als solche kenntlich gemacht habe.

Graz, am …… ……..

(Unterschrift)

Englische Fassung:

STATUTORY DECLARATION

I declare that I have authored this thesis independently, that I have not used other than the declared sources / resources, and that I have explicitly marked all material which has been quoted either literally or by content from the used sources.

…… ……..

date (signature)

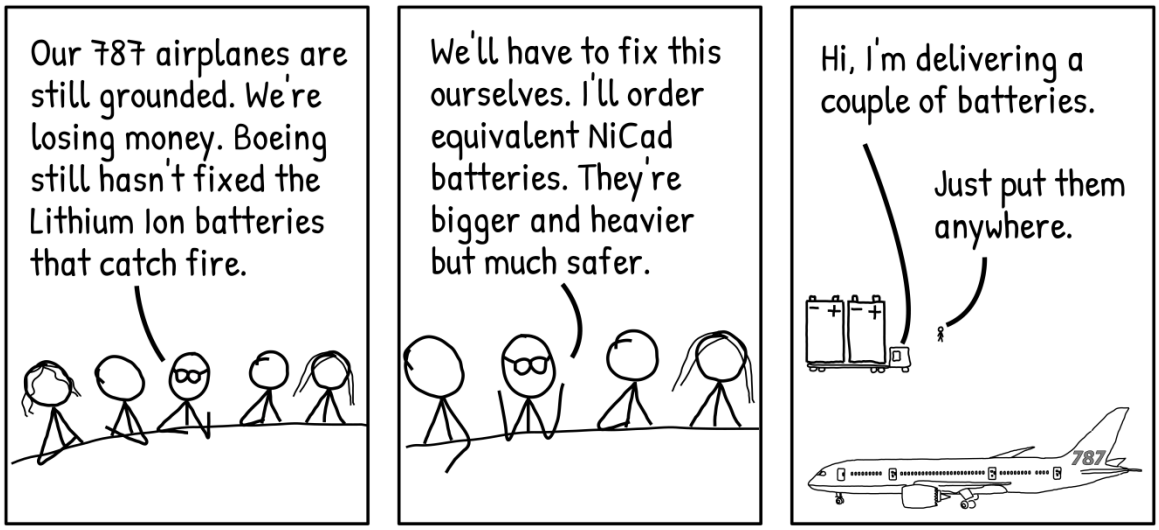

Boeing 787 Batteries.

Acknowledgements

I am using this opportunity to express my gratitude to everybody who encouraged and supported me during my studies and the development of this thesis.

Primarily, I would like to thank Prof. Frank Uhlig and Dr. Ilie Hanzu for the provision of an interesting topic and giving me the opportunity to work on it. They supported me throughout the master thesis by giving advice and encouragement, as well as invaluably constructive criticism whenever needed.

I want to thank all members of both research groups, AG Uhlig and AG Wilkening, for their cooperativeness and the enjoyable atmosphere created by them, which contributed a lot towards the outcome of this work. Especially I´d like to thank Cathrin Zeppek for her mental and active support during our cooperation. Also the advice of Judith Binder, Stefan Müller, Pierre Baumann, Michael Haas and Ana Torvisco as well as the enjoyable talks with my office colleagues Judith Radebner and Vera Dopona were priceless to me. I´d like to acknowledge Astrid Falk and Melanie Wolf for the GC-MS measurements and Monika Filzwieser for providing everything needed for the experiments, be it chemicals, advice or elementary analysis measurements.

Additionally, I want to thank my friends who have always been there for me during the past years in every (im-)possible situation. Their company, encouragement, patience and constructive criticism sweetened this time a lot. Especially my closest friends, Rahel Beuchel, Bettina Grumm, Lukas Schafzahl, Felix Anderl and Yasmin Bürkl always lent me an ear and supported me wherever possible.

Above all, my thanks go to my parents Susanna and Rolf as well as to my sister Christina for supporting me in every way possible and thus giving me the opportunity to pursue these studies. Thank you for your constant advice, sympathetic ears and distraction when needed. Without you, my studies would not have been possible.

Furthermore, an extraordinary role was played by my boyfriend Daniel Erhart, who went through thick and thin with me during the past ten years. Thanks to his loving support and ability to calm me down whenever necessary, I have been able to achieve many of my goals.

Abstract

In this work mainly the influence of octaphenyl-cyclotetrasilane (Si_4Ph_8) and decaphenyl-cyclopentasilane (Si_5Ph_{10}) on the capacity of graphite in lithium-ion half-cells has been tested. For this purpose, the silanes were pretreated differently depending on the preparation procedure of the electrodes used. Pretreatments included pyrolysis of the silanes, mixing and/or ball-milling of the same with graphite, polymeric binder, carbon and solvent. Also, first experiments on the influence of aryl-substituted stannanes such as mesityltin trihydride ($MesSnH_3$) or naphthyltin trihydride ($NaphSnH_3$, with and without *in situ* polymerization by the amine base tetramethylethylenediamine (TMEDA)) and perphenylated germanium rings (octaphenyl-cyclotetragermane Ge_4Ph_8, decaphenyl-cyclopentagermane Ge_5Ph_{10}) on the capacity of graphite were performed. Furthermore, synthesis of dichloro-(1-naphthyl)(phenyl)silane as a precursor material to cyclic polysilanes was conducted.

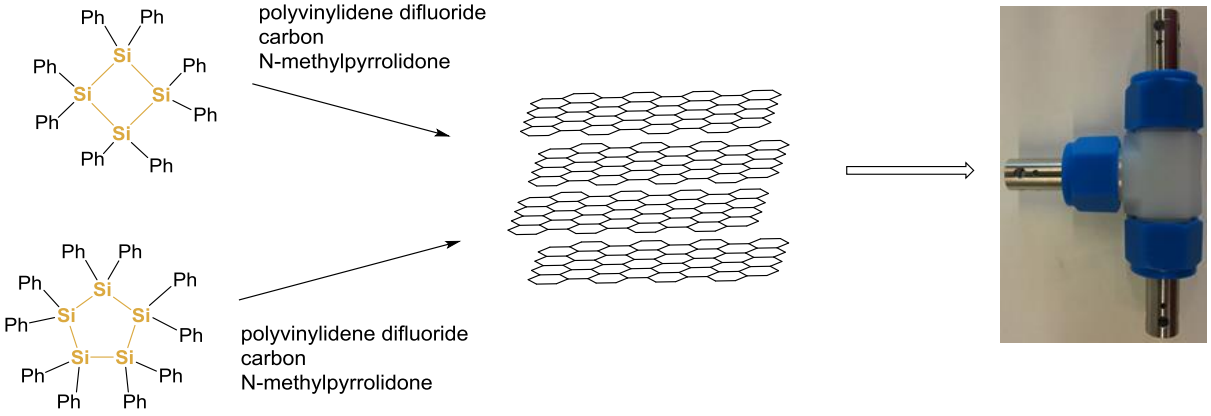

Zusammenfassung

Im Zuge dieser Arbeit wurde der Einfluss zweier zyklischer Silane (Octaphenyl-cyclotetrasilan Si_4Ph_8 und Decaphenyl-cyclopentasilan Si_5Ph_{10}) auf die Kapazität von Graphit in Lithium-Ionen Halbzellen untersucht. Dazu wurden die Silane entsprechend des Präparationsverfahrens der verwendeten Elektroden unterschiedlich vorbehandelt. Die Vorbehandlungen inkludierten Pyrolyse der Silane, Mischen und/oder Mahlen derselben mit Graphit, Binder, Leitruß und Lösungsmittel. Zudem wurden auch erste Untersuchungen zum Einfluss von aryl-dekorierten Stannanen, darunter Mesitylzinntrihydrid ($MesSnH_3$) sowie Naphthylzinntrihydrid ($NaphSnH_3$, vor sowie nach einer *in situ* Polymerisation mittels der Amin Base Tetramethylethylendiamin (TMEDA)), sowie von perphenylierten Germaniumringen (Octaphenyl-cyclotetragerman Ge_4Ph_8 und Decaphenyl-cyclopentagerman Ge_5Ph_{10}) auf die Kapazität von Graphit durchgeführt. Des Weiteren wurde Dichlor-(1-naphthyl)(phenyl)silan als Vorstufe zu einem entsprechenden zyklischen Polysilan synthetisiert.

Table of contents

1 Introduction

Along with the rapid research and development of new technologies over the last decades, such as electric vehicles and portable electronic systems, a need for long cycle-life, high-capacity batteries has coevolved. These batteries have to meet various prerequisites, including high rates of charge/discharge as well as high energy density. The realization of such batteries requires the use of electrode materials with a high specific capacity, for instance the light metals Li, Na, K and Mg. Even though these metals show a high theoretical capacity, their direct utilization as active anode materials in rechargeable batteries is in most cases dangerous, since it is often accompanied by spontaneous reactions when in contact with an electrolyte caused by the strong reducing power of the metals. Starting in the early 1980s, the lithium metal was replaced by lithium insertion materials.[1] Lithium-ion (Li-ion) technology is since being optimized by usage of various alternative insertion host materials. Currently, the most used Li-ion battery technologies use graphite as active anode, which is capable of hosting of lithium ions between its layers. Li-ion batteries and all their components ought to be able to fulfil several crucial criteria of different natures. High energy and power density, durability and long life time are deemed as important as low cost and safety aspects. To date, for all of the above requirements graphite represents the best compromise. Thus, unsurprisingly, graphite is the most frequently used anode active material.

As a disadvantage, graphite operates at an upper theoretical limit of 372 mAh g^{-1} whereas the theoretical capacity of lithium metal is 3860 mAh g^{-1}.[2] Intensive research on various approaches towards increasing the capacity of anode materials and of Li-ion batteries in general is being conducted. One of these approaches involves insertion of high-capacity heteroatoms, such as silicon, germanium or tin, into the layers of graphite and is dealt with over the course of this work. Silicon has a long history of investigation, owing to its unparalleled high theoretical capacity of 4200 mAh g^{-1}, its low cost and raw material abundance.[3] Nevertheless, this huge capacity comes with the disadvantage of a high volume expansion (nearly 400 %) during the electrochemical lithiation process, which results in a rapid loss of capacity upon cycling and hence very poor cycle life. The problem of volume expansion has been somehow circumvented by the usage of nanostructured silicon. The fabrication of such nanostructures may be achieved by two possible technological approaches: top-down methods, where elemental silicon is being milled or in any other way treated to form (nano)particles, or bottom-up methods, where the nanostructures are built starting from a molecular level. In this work, a variant of the latter method (bottom-up) was studied. The work started with the testing of four- and five-membered perphenylated silicon rings in Li-ion half-cells and synthesis of similar cyclopolysilanes with larger aromatic substituents. The perphenyl cyclopolysilanes are of special interest due to their ability to electrochemically form radical anions[4]

with the delocalized extra electron within the silicon skeleton. The influence of these radical anions in combination with the aromatic substituents is likely to contribute to a higher capacity of graphite if mixed with the aforementioned compounds.

2 Literature Overview

2.1 Lithium-Ion Batteries: General Approach

Battery cells may be classified in three groups: primary cells, secondary cells and fuel cells. Primary cells consist of materials that are consumed during the irreversible electrochemical reaction and hence are non-rechargeable. A prominent example for a primary cell is consisting of copper and zinc, known as the Daniell element. Li-ion batteries are classified as secondary cells or accumulators, in which reversible electrochemical reactions take place.[5] After a discharge of the cell, a reversion of the process is forced by an externally applied electrical energy and hence delivers the reactants in their original form again. A reversibility of hundreds or thousands of cycles and therefore prolonged lifetime is an advantage not only in acquisition costs but also concerning environmental factors, as less material has to be used. Generally, Li-ion batteries consist of lithium, often containing a transition metal oxide, as positive electrode material and a carbonaceous material as negative electrode. Upon assembly of the cell it is in discharge state. When charged, electrons move from the cathode to the anode through an external circuit with the charger and lithium ions vice versa (Scheme 1). The cell-voltage increases as the potential of the cathode rises and that of the anode is lowered during the charging step. This voltage may be used as power source during the discharging period.[6]

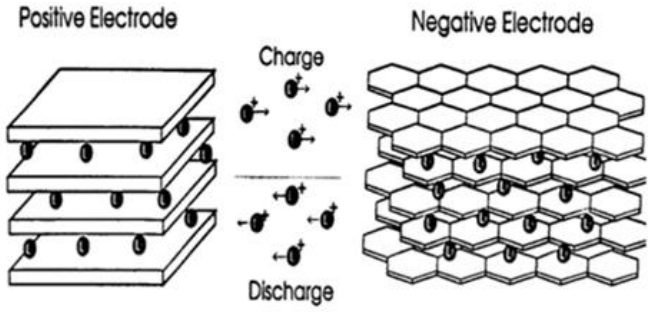

Scheme 1: Charge and discharge of a Li-ion battery*

In the past decades, various alternative materials for negative electrodes have been used and widely investigated. The utilization of the light metals Li, Na, K and Mg as negative electrodes with exceptional negative standard redox potential was avoided, as they tended to cause a sudden release of the high amount of stored energy, probably triggered by the contact with an electrolyte.[7] Also

* http://www.digikey.com/en/articles/techzone/2012/sep/a-designers-guide-to-lithium-battery-charging, 22.10.2014

local heating to a temperature above the melting point of the corresponding material causes a detonation of the battery. These explosive incidents, all related to the negative electrode, generated an additional demand for safety in portable accumulators. Thus, the use of carbonaceous materials with closest-packed hexagonal structures as anode material in Li-ion batteries has been widely spread. Especially graphite received much attention, as it offers many advantages, being light weight, having high crystallinity and the possibility of ion storage between its layers. The structure is composed of hexagonally arranged carbon atoms, stacked in a highly orderly fashion. These so-called graphene layers are held together by weak Van der Waals forces. Different forms of stacking of graphite are known, being ABABA... hexagonal graphite and ABCABC… rhombohedral graphite (Scheme 2) whereas the latter appears less often i.e. as small part of the solid. The distance perpendicular to the layer planes is 0.3354 nm, while the carbon-carbon bond parallel to the layer planes is 0.142 nm. Moreover, the crystalline structure of graphite proved to cause anisotropic physical properties, such as the electrical conductivity which is 100 times higher in parallel direction to the basal plane than it is in perpendicular direction.[8]

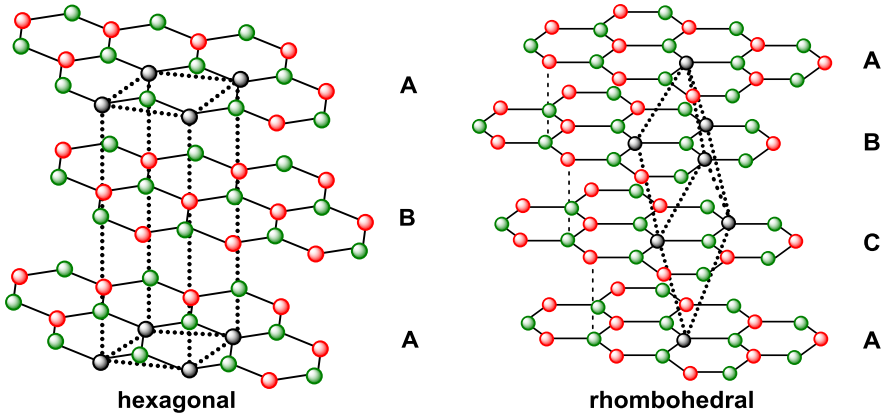

Scheme 2: Hexagonal and rhombohedral stacking of graphene layers

Graphite has two specific surfaces present, the basal plane and the edge sites. They provide a target for ion migration and thus enhance the conductivity of Li-ion batteries. The graphitic anodes are able to be electrochemically inserted with Li-ions in a process called lithium insertion or intercalation.

2.1.1 Intercalation of Lithium into Graphite

2.1.1.1 Intercalation in General

In 1955, Hérold reported first formation of lithium-graphite intercalation compounds (Li-GIC´s), of the formula Li_xC_n by chemical synthesis.[9] In highly crystalline graphite at ambient pressure, a maximum lithium content of one lithium ion per six host carbon atoms is attainable (with Li_xC_n, $x \leq 1$ and $n \geq 6$). The intercalation of Li-ions into graphite proceeds according to the general reaction scheme.[7]

$$Li_xC_n \underset{\text{charge}}{\overset{\text{discharge}}{\rightleftharpoons}} xLi^+ + xe^- + C_n$$

The lithiated carbon Li_xC_n is formed during the electrochemical reduction (charge step) by pervasion of the lithium ions from the electrolyte along the edges, defect sites or prismatic surfaces of the graphite. During the intercalation step, due to the volume of the inserted guest ions, the distance between the graphene layers increases to 0.370 nm (10.3 % for LiC_6, calculated by Song, Kinoshita and Tran[10]) and the energetically favored stacking order of the graphene layers changes to AAA…, where the layers are stacked congruently.[11] In this stacking order, two adjacent graphene layers face each other directly.

2.1.1.2 Stage Formation

In general, given a low concentration of guest species, lithium intercalation forms a periodically ordered array of unoccupied layer gaps, called stage formation.[9] This process occurs stepwise and a stage index *s* was introduced, which equals the number of unoccupied graphene layers between the two closest lithiated layers. This staging phenomenon is thermodynamically driven and correlates to the amount of energy that is necessary to "open" the existing Van der Waals gap just enough to let a guest ion enter between the graphene layers. The effect of the repulsive coulombic forces between the lithium guest ions proves to be less effective than the driving force to occupy the graphene layers in orderly fashion. Subsequently, only few but nevertheless highly occupied Van der Waals gaps are energetically preferred over random distribution of the Li ions.

In order to observe staging phenomena as well as the degree of intercalation, galvanostatic (at constant current) reduction of graphite to LiC_6 in a Li-containing electrolyte was performed. LiC_6 corresponds to a lithium storage capacity of 372 mAh g^{-1} with respect to the graphite mass. During the reduction, emerging plateaus are observable. These were assigned to two-phase regions, where two phases coexists.[12]

Scheme 3 shows the simplified stage formation during the electrochemical lithiation of graphite and formation of Li_xC_n, as drawn by Winter and Besenhard.[15] The stages refer to the amount of Li-ions in in graphite for Li_xC_6. Due to different stacking behavior at temperatures between 10 °C and 700 °C and therefore lithium density, stage II was divided into two parts: s = II (where x = 0.5) and s = II L (where x = 0.33). Below this temperature limit, it was reported to disappear[12], above it the $Li_{x'}C_6$ phase with $0.5 \leq x \leq 1$ is converted into lithium carbide Li_2C_2 and carbon.[13] Many stages of $s > II$ were reported, even some higher than $s = IV$, but the reported literature on the staging process contain discrepancies, which are discussed by Imanishi.[14]

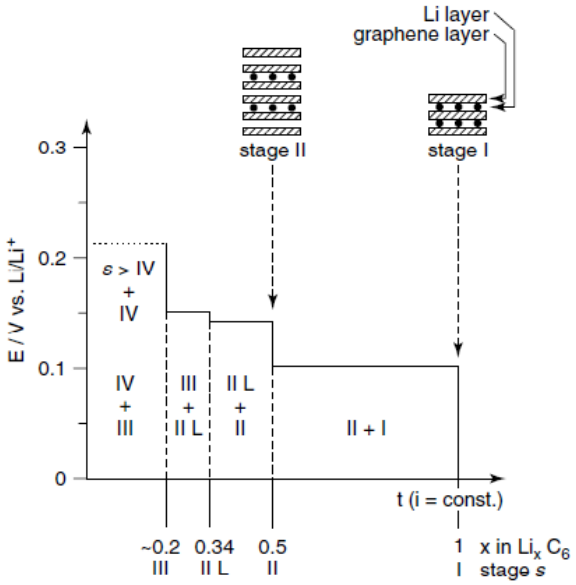

Scheme 3: Simplified stage formation during the electrochemical formation of Li_xC_6[15]

Investigations on the influence of hexagonal or rhombohedral structure of graphite on the stage formation mechanism and the storage capacity - induced by the fact, that commercial graphite contains both -, came to the conclusion, that both behave similarly.[16]

2.1.1.3 Influence of Li-intercalation on the (ir)reversible Specific Charge

In theory, the Li intercalation into graphite should be fully reversible. Practically, a charge consumption of more than the theoretical specific charge of 372 mAh g^{-1} is observed during the first cycle of an experimental charge/discharge curve. The subsequent delithiation of the graphite matrix only recovers about 80-95 % of this charge. In the following cycles, no such behavior was evident, but rather lower charge consumption for the lithiation step and almost complete charge recovery during delithiation.[17] This occurrence was accredited to the formation of a solid electrolyte interphase (SEI), which kinetically protects the thermodynamically unstable electrolyte from further reduction on the lithiated graphite surfaces. This film formation happens through a charge consuming side-reaction in the first few intercalation/de-intercalation cycles with most of the film actually forming during the first reduction of the graphite. First, the most unstable components of the electrolyte with respect to reduction react selectively, which results in an accumulation of decomposition products at the SEI on the graphite and therefore a loss of capacity. Additionally, the graphite electrode is being passivated by the SEI throughout the cycling process. The SEI formation on lithiated graphite is correlated to irreversible material consumption. Therefore, corresponding charge loss is called “irreversible capacity” or “irreversible specific charge”.[7] These losses have been subject to various investigations, since any irreversible reaction implies an additional material expense.

Insertion of lithium is also possible in other highly ordered host lattices, such as silicon. Due to its high, unmatched theoretical capacity of 4200 mAh g^{-1}, it gained much interest over the last decades.

2.2 Silicon, Germanium and Tin

2.2.1 General Aspects

Silicon, germanium and tin are promising candidates for anodes in Li-ion batteries, as they are able to form several alloys by electrochemically incorporating large amounts of lithium. Their theoretical capacities exceed by far the capacity of fully lithiated graphite (372 mAh g^{-1}), reaching values of 4200 mAh g^{-1} for Si,[18] 1625 mAh g^{-1} for germanium,[19] 1491 mAh g^{-1} for tin-oxide[20] and 991 mAh g^{-1} for pure tin,[21] respectively. In spite of this significant capacity advantage, these materials have a non-negligible problem: they undergo a major volume change during lithiation/delithiation reactions. In case of silicon, the volume change accounts to approximately 400 %, for germanium 370 %. This volume expansion in charge and subsequent contraction in discharge causes cracks and pulverization of the active materials and loss of electrical contact in the electrodes leading to a quick fading of the capacity. A possible solution was found by using nanoparticles, as they are small enough when properly spaced, to allow the phenomenon of "active material breathing" (i.e. the volume expansion and contraction of active materials upon cycling described above) to take place without the occurrence of stress and strain that breaks down a normal (not nanosized) electrode.

2.2.2 Nanocomposite Materials

In recent research, different methods have been applied to combine the best qualities of carbon and silicon, as it seems to hold the most advantages of the mentioned group 14 metals. One of these methods contains coating of nanostructured metals with a layer of a carbonaceous material.[22] Chemical/thermal vapour deposition (CVD/TVD) of the silicon component on the charge-collector material is also a frequently used method for anode preparation. Another comprises the formation of a Si/C nanocomposite material by decomposition of organic precursors (pyrolysis) or usage of high-energy mechanical milling or a combination of both.[23] In any case, the testing of such anodes proved that the preparation of the electrodes is the key to well-functioning battery-cells.

Alhough similar methods may be applied to germanium and tin as well, also with considerably improved capacity values, the main focus of current research lies on silicon nanocomposite materials.

To the best of our knowledge, so far, no information about cyclic silanes as anodes for Li-ion batteries is available. In this work, first experiments on the usage of perphenylcyclopolysilanes incorporated into a graphite matrix as anode for Li-ion batteries have been conducted. The materials were mostly studied by two common electrochemical techniques: Galvanostatic Cycling and Cyclic Voltammetry. Additionally, first qualitative tests of aryl-substituted tin hydrides as well as perphenylated cyclopolygermanes were carried out by Cyclic Voltammetry.

2.3 Perphenylcyclopolysilanes

2.3.1 General Approach

Perphenylcyclopolysilanes have first been investigated in 1921 by Kipping and Sands.[24] In this early state of research, Kipping provided fundamentals on perphenylated cyclopolysilanes. He postulated a finding of different silicon species which he called compounds *A*, *B* and *C*. In this work, structures for each compound were suggested according to rough approximation of melting points, behaviour in different solvents and elementary analysis (Scheme 4). For *A* an "unsaturated" silicohydrocarbon of the formula Si_4Ph_8 with a melting point of roughly 335 °C was proposed. In later research, the melting point of *A* was more accurately determined to be 321-323 °C and the currently known structure in form of octaphenylcyclotetrasilane (further referred to as Si_4Ph_8) was introduced.[25] The substance was found to be sparingly soluble except for in boiling aromatic solvents such as aniline, benzyl alcohol and phenol.[24] Keeping these solutions boiling for some time resulted in decomposition.

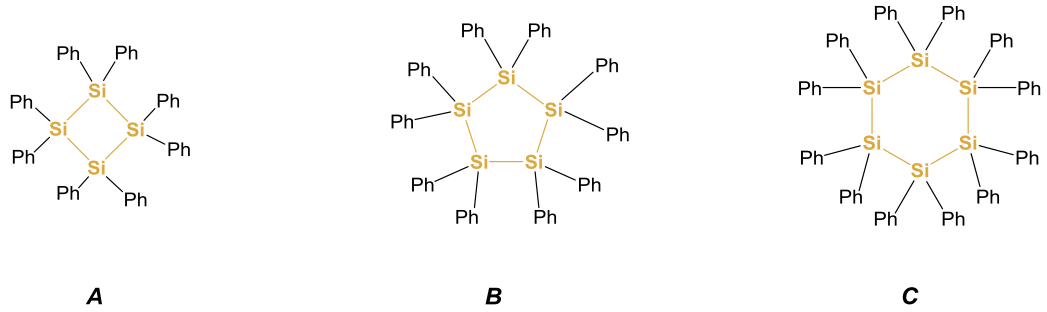

Scheme 4: Chemical structure of perphenylated silicon rings containing 4, 5 and 6 silicon atoms

For *B* a "saturated" silicohydrocarbon was assumed, also according to the formula Si_4Ph_8, with an estimated melting point of more than 400 °C. In comparison to substance *A*, *B* proved rather inert while being treated with an excess of iodine or bromine. Also a repeated recrystallization from different boiling solvents did not lead to decomposition of the substance. In later research dedicated to compound *B* performed by Gilman,[26,27] two different compositions were proposed. The first alternative was based on molecular weight determinations to indicate a dodecaphenyl cyclohexasilane (Si_6Ph_{12}). In the second postulation[27], the existence of decaphenyl cyclopentasilane (further referred to as Si_5Ph_{10}) was proved by different methods including X-ray diffraction, ebullioscopic measurements and elementary analysis.

2.3.2 Properties of Perphenylcyclopolysilanes

These perphenylcyclopolysilanes have attracted attention since their discovery not leastly considering their different behaviour from the known carbon analogues. Contrarily to the latter, electron delocalization effects similar to aromatic organic rings are revealed by cyclopolysilanes. This effect, however, should be interpreted by σ-delocalization rather than π-bonding like in organic aromatic rings.[28] Additionally, cyclopolysilanes show the ability of forming charge transfer complexes

as well as a reducibility to form radical anions. The latter phenomenon was studied by Hengge in 1979[4] by electron spin resonance spectroscopy (ESR). Therefore he generated radical anions using the standard procedure involving sublimed potassium under high vacuum as well as an electrolytic reduction. It was observed that contrary to Si_5Ph_{10} an electrochemical reduction of Si_4Ph_8 was not possible. According to the resulting ESR spectra several conclusions were drawn. Radical anions of both the four- and the five-membered perphenylcyclopolysilanes are stable at low temperatures. The reduction does neither result in cleavage of perphenylated Si-Si bonds,[29] nor in generation of secondary anion radicals as observed by Wan.[30] Another observation suggested a delocalization of the extra electron within the Si_n ring and the surrounding cylinder of the 2*n* phenyl ring α carbons rather than into the phenyl groups. Comparison between the ESR spectra of the four and five membered perphenylcyclosilane also indicated a similar and possibly planar structure of the respective radical anions $[Si(C_6H_5)_2]_4^{\cdot -}$ and $[Si(C_6H_5)_2]_5^{\cdot -}$.[4]

Further, the ring size of cyclopolysilanes is dependent on the size of their substituents. In case of the perphenylated cyclopolysilanes, ring sizes of 4 – 6 Si atoms are preferred. Even though Si_4Ph_8 exhibits a high ring strain and therefore a higher reactivity than its larger counterparts, it is a scarcely soluble, stable compound. On the other hand, the high stability of Si_5Ph_{10}, which melts at 464 °C without decomposing, is possibly caused by low ring strain and steric protection of the Si skeleton by the phenyl groups.[28]

Electrochemical properties of perphenylated cyclopolysilanes have been investigated only superficially in context of electrochemical oxidation using Cyclic Voltammetry.[31]

2.3.3 Synthesis of Perphenylcyclopolysilanes

Synthesis of octaphenylcyclotetrasilane was reported to be successful *via* different routes. Kipping used Wurtz type coupling of diphenylsilicon dichloride, heated with an excess of sodium which resulted in three different crystalline compounds (2.3.1). The thermodynamic equilibrium is rapidly reached if the alkali metal is used in excess.

The other route of synthesis is *via* electrochemical reduction, where a reductive elimination of halides occurs. This was investigated by Hengge and Firgo,[32] who used a solution of tetra-*n*-butylammonium perchlorate (TBAP) and diphenyl dichlorosilane in 1,2-dimethoxyethane (DME) to which voltage was applied. After a reaction time of 12 h, the insoluble product was formed to give 100 % yield in form of cathodic precipitate.

2.3.4 Chemical Reactivity

In general, ring opening reactions were observed for several strained cyclotetrasilanes, including Si_4Ph_8. A reaction with lithium results in cleavage of the octaphenylcyclotetrasilane. This reaction leads to dilithium-octaphenyltetrasilane which crystallizes with tetrahydrofuran (THF) molecules.[33] Another reaction of cyclotetrasilanes is the anionic ring-opening polymerization which, in case of

Si_4Ph_8, leads to a rearrangement to Si_5Ph_{10} as the only product. The lesser strained decaphenyl-cyclopentasilane may be cleaved by lithium as well. Depending on the reaction conditions, this cleavage results in different lengths of dilithio silicon chains. Cleavage of the silicon ring was also observed to occur through electrochemical oxidation after the formation of the corresponding cyclosilanes cation-radicals.[31]

2.4 Aryl substituted Tin Compounds

Aryl substituted tin compounds such as mono-, di- and trihydrides pose interesting candidates for graphite composite anodes in Li-ion batteries. These hydrides are air-sensitive and decompose easily at room temperature under disproportion and formation of metallic tin.[34] Their stability is depending on the size and number of the substituents. The reactivity of these compounds proved advantageous for polymerization reactions, which are often started by usage of bases such as tetramethylethylenediamine (TMEDA) and most likely include a radical mechanism.[35] The exact mechanism, however, is not yet completely understood. Different aryl-substituted tin trihydrides, including *o*-tolyl, mesityl, 2,4-xylyl, 2,6-xylyl and naphthyl, have been prepared, polymerized and characterized by C. Zeppek.[36,37] Characterisation included a high resolution scanning electron microscopy (HR-SEM) investigation of the polymerized particles (e.g. for *o*-tolyl derived from diethyl ether (Et_2O), Figure 1). Instead of the usual polymeric chains of covalently bonded metal, these polymers display a core-shell structure. Even though this structure is yet only known for the *o*-tolyl derivative, a similar behaviour is feasible for other aromatically substituted tin hydrides.

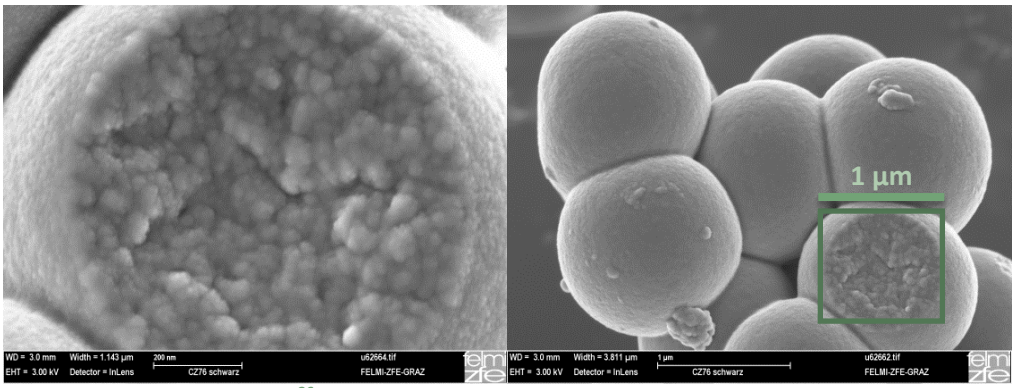

Figure 1: HR-SEM (*o*-tolylSn)$_n$ from Et_2O[36]

In 1996, Tanaka[38] found that tin radicals may also be electro-generated, and a subsequent polymerisation is possible by an electrochemical initiation of tin hydride promoted radical chain reactions. The generation of radicals is easily possible under mild conditions due to the very weak Sn-H bond. In this work, the influence of tin trihydrides as such, as well as in their polymeric form (preformed or *in situ* preparation) on the electrochemical activity of graphite in Li-ion batteries was tested.

3 Results and Discussion

3.1 Characterisation of the Silicon Rings

During this work different samples of perphenylated cyclosilanes (Si_4Ph_8, Si_5Ph_{10} and a sample of unknown composition Si_xPh_y) were examined with respect to their electrochemical features. The materials were also characterised using NMR and Raman spectroscopy. The resulting data indicate for the unknown sample of Si_xPh_y a mixture of both, Si_4Ph_8 and Si_5Ph_{10}.

3.1.1 NMR Spectroscopy

^{13}C and ^{29}Si NMR spectroscopy in $CDCl_3$ or C_6D_6, respectively, was performed on the silicon containing samples used in this work. The chemical shifts found are listed in Table 1.

Table 1: NMR shifts of the silanes

	^{13}C	^{29}Si
Si_4Ph_8	δ = 127.6, 128.7, 135.1, 137.2 ppm	δ = -22.0 ppm
Si_5Ph_{10}	δ = 127.7, 128.7, 134.9, 138.3 ppm	δ = -34.2 ppm
Si_xPh_y	δ = 127.4, 128.5, 134.4, 137.8 ppm	δ = -21.7 (very weak signal), -34.6 ppm

3.1.2 Raman Spectroscopy

Raman spectroscopy has been conducted for each variation of the silicon ring-systems. As a reference, data from D. Kovar[39] was used as shown in Table 2. Since the spectra of analogous cycles are identical in the region of 4000 - 800 cm^{-1}, only the long-wave area (800 - 100 cm^{-1}) is being shown below (Figure 2).

Table 2: Raman spectroscopy data (s = strong, m = medium, w = weak, sh = sharp, v = very)

	Peaks
Si_4Ph_8 [39]	184 (s), 208 (s), 244 (s), 430 (w),453 (w), 486 (w), 539 (m), 550 (s), 622 (m), 689 (w), 708 (w), 744 (vw)
Si_4Ph_8	157 (w) 179 (s), 189 (w), 204 (s), 240 (s), 426 (w), 450 (w), 472 (vw), 483 (w), 537 (s), 548 (s), 619 (s), 685 (w), 704 (w), 740 (vw)
Si_5Ph_{10} [39]	162 (vs), 179 (s), 210 (s), 245 (m), 372 (w), 442 (w), 510 (sh), 517 (s), 532 (sh), 618 (m), 684 (m), 737 (w)
Si_5Ph_{10}	163 (vs), 176 (s), 182 (s), 197 (m), 210 (s), 245 (m), 372 (w), 441 (w), 510 (sh), 520 (s), 532 (sh), 550 (s), 619 (m), 685 (m), 738 (w)
Si_xPh_y	163 (vs), 177 (s), 194 (m), 211 (m), 244 (m), 372 (w), 511 (m), 522 (s), 535 (w), 549 (m), 620 (s), 685 (s), 706 (vw), 737 (w), 785 (w)

According to these data, the unknown sample Si_xPh_y is likely to be a mixture of both, the four- and the five-membered silicon ring. Due to a lack of the sample, an isolation of the rings was not possible. It is not unlikely, that this mixture contains a cleaved product in form of a poly(diphenyl)silane.

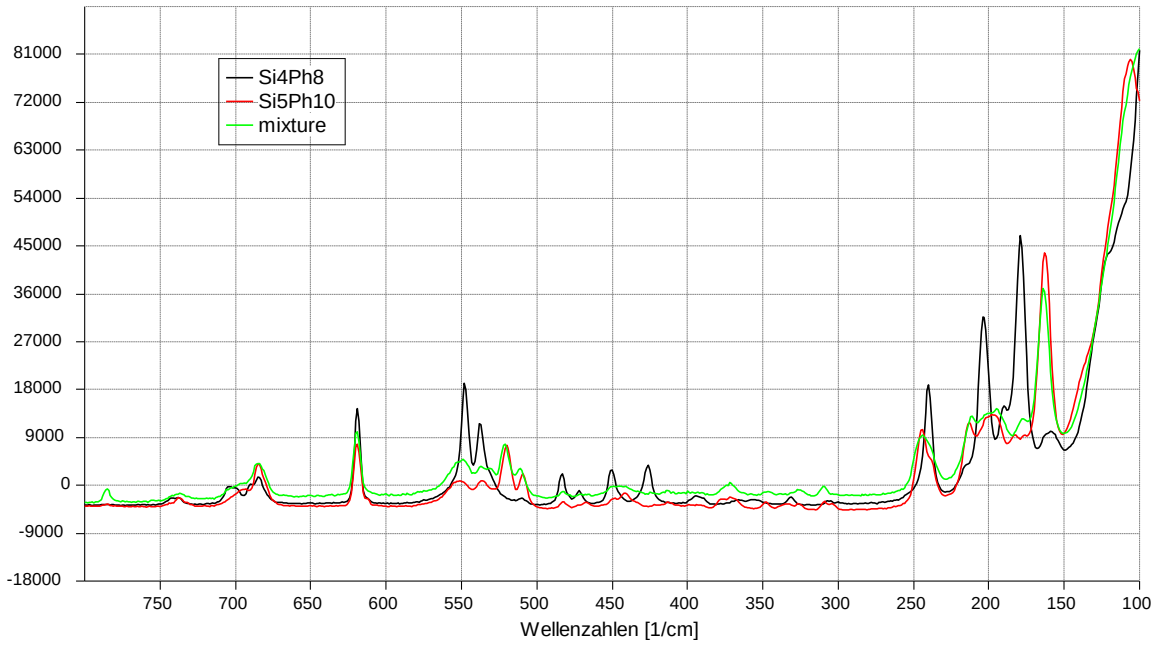

Figure 2: Raman spectra

3.1.3 Elementary Analysis

Elementary analysis was performed on a vario EL III from *elementar* with CHN element analyser. Combustion of the samples occurred at 1200 °C. The small amounts of nitrogen for the pyrolysed sample result from adsorption to the surface during the storage in the glove-box. Since the untreated perphenyl cyclopolysilanes are stable at air, storage in the glove-box was not necessary and no nitrogen appears in the measurements. Regarding previous characterisation of the untreated samples, the remaining percentage not covered by carbon and hydrogen was assigned to silicon. Assuming the same for the pyrolysed samples, following percentages result from the measurements (Table 3).

Table 3: Elementary analysis results of the (pyrolysed) perphenylated cyclosilanes

	C [%]	H [%]	Si [%]	N [%]
Si_4Ph_8	78.78	5.48	15.74	-
Si_5Ph_{10}	78.45	5.49	16.06	-
Si_4Ph_8 (pyrolysed)	69.95	1.64	27.88	0.53
Si_5Ph_{10} (pyrolysed)	70.57	1.62	27.21	0.60

Pyrolysis causes an opening of the silicon ring system and cleavage of some of the phenyl groups. Gas Chromatography Mass Spectroscopy (GC-MS) analysis of the residues in the combustion oven shows larger amounts of diphenylsilane (14 %), triphenylsilane (35 %), tetraphenylsilane (15 %) and 9,9-diphenyl-9H-9-silafluorene (7 %) likewise. According to elementary analysis of the pyrolysed products, the silicon content of the sample almost doubles in contrast to a drastically sinking of the amount of hydrogen in comparison to the untreated cyclosilanes. This further indicates a ring-opening of the phenyl groups to a certain extent. Also an early formation of silicon carbide (SiC)-species is possible.

3.2 Experimental Errors and how to prevent them

An important issue related to the assembly of batteries with different materials is not only to reach a high capacity and cyclability, but also a reproducibility of the experiments and the errors in experimental determinations of key parameters. During the preparation of the electrodes, various error sources significantly influencing the recorded behaviour of the materials in the test-cells are being encountered. Some of them include purity of the chemicals, homogeneity of the created slurries, evenly or non-evenly cast films and equal heat distribution during the drying process, to name a few. In this work, different methods and compositions have been tested in order to create reproducible data and narrowing down the errors to a minimum.

3.2.1 Preparation of Electrodes

Purity of the chemicals is one of the crucial requirements for a well working electrode. Every trace of impurity will show an effect on the battery that can be identified on the resulting measurements only with some difficulty. To avoid this kind of errors, purification of industrially produced chemicals is often inevitable. In case of solids, recrystallization with pure solvents or sublimation of the chemicals may be conducted. Depending on the preparation method and the air-/moisture-sensitivity of the compounds, a distillation and drying of used liquids over a column-system with subsequent storage over molecular sieve to prevent impurities and traces of water should be considered.

A lack or improper cleanliness of the equipment is the next source of contamination. For the preparation of electrodes, and later on the assembly of the cells, different tools are being used: polyethylene (PE) vials with lid, spatulas, stirring bars, metal foils, tweezers, gloves, casting blades and the working space itself. All of the above mentioned should be cleaned thoroughly before usage; gloves should be exchanged if a contamination occurs. Even though it often is a negligible cause of errors, touching of the surface of any tool without gloves, that later-on comes in touch with the sample, leaves a trace of lipids and salts from the human skin on the surface, which might be transferred to the electrode.

The accuracy of the results (determination of current, capacity or other parameters) is widely dependant on the accuracy of the balances used. A reference should be weighed several times beforehand to estimate the average errors caused by inaccuracy of the device. Also triple or multiple determinations of the electrodes after drying proved useful in later estimations of errors. Variance of 0.2 % was observed for the precision five-decimal analytical balance used. In case of air-sensitive samples, where the weighing needs to be carried out in the glove-box, accuracy is not surprisingly low (up to 7 % dispersion for one sample) due to recirculation of the atmosphere and the variable pressure, and thus buoyancy of the balance parts, unavoidably caused by the user that handles the sample in the glove-box. Additionally, a slight vibrating motion of the glove-box due to the connected

vacuum pump and other parts cause inaccuracy of the balance. Therefore, all experiments conducted for air-sensitive compounds provide rather qualitative than quantitative information.

Homogeneity and composition are other key aspects on the way towards fully functional Li-ion electrodes. The homogeneity of the original slurry may be controlled by the stirring rate. In this thesis, a stirring rate of 600 rpm was chosen for all experiments. The centripetal forces cause a diffusion of the components in the slurry; therefore an appropriate placing on the magnetic stirrer is required. If these requirements are not met, an agglomeration of particles will cause irregularities on the surface of the electrodes later. Also the binding polymer is likely to coat graphite-particles, inhibiting its electrochemical activity. This effect is obviously dependent on the amount of polymer used: with increasing amount of polymer, a larger dispersion of the resulting capacities may be observed. Homogeneity is also widely influenced by casting of the slurry onto the metal foil. Thus, a flat surface and an even casting are required. The first requirement is usually achieved by using a casting table connected to an adequately strong vacuum pump. A homogeneous surface may be accomplished by avoiding any form of ripples or curling of the metal foil. For that purpose, a clean paper and tissue might be used to spread the metal foil evenly over the in-built vacuum-ports of the casting table. It is necessary to ensure, that the casting blade does not show irregularities and is able to proceed evenly over the foil without touching and scratching it. Usually, only negligible grooves will remain on the surfaces which are evening out along with the evaporation of the solvent during the drying process.

The thickness of the cast layer, governed by the size of the casting gap, also largely influences the homogeneity. With increasing layer thickness, an uneven drying process will occur in the oven, starting from the sides proceeding to the thickest part of the film, evolving gas-bubbles in the meantime. In case of thick films, the material is more likely to crackle and expose the foil underneath. Both occurrences largely disturb the function of the electrodes. Crackling of the coating is also likely to happen during the cutting of the electrodes, if insufficient binder was added. The resulting film thickness is not only influenced by the choice of casting gap but also by the viscosity of the slurry. A balance needs to be met, where the slurry is liquid enough to be spread easily but viscous enough to stay in place.

3.2.2 Assembly of Swagelok®-Cells

For the Swagelok®-cells it is very important that they are being cleaned and dried properly to avoid side-reactions caused by previously used chemicals. Usually the plastic parts are rinsed extensively with deionized water, isopropanol and/or acetone. Cleaning of the steel parts occurs in water, ethanol and acetone in an ultrasonic bath for at least 15 min in three separate steps. All parts are dried with a paper towel and put into an oven at 60 °C for at least 3 h before usage.

During the assembly, various factors can lead to non-functional test-cells: contamination, short circuits and leaky cells. The main source of contamination are the gloves themselves from the glove-box, thus usage of an additional layer of single use latex gloves is recommendable. In order to prevent other contaminations, clean tools and work space (i.e. by usage of a new placemat) have to be used without exception.

Since the surface of the lithium band used for the electrodes will likely oxidize due to some solvent vapours present within the glove-box atmosphere, its top layer needs to be removed using a scalpel. This removal procedure may sometimes leave and spread particles of lithium on the electrodes, separators, cell parts etc. which may affect the functionality of the cell or in an extreme case even lead to a short circuit. Thus special care has to be taken to avoid metal (lithium) particle contamination. Another malfunction is possible by leaving gas bubbles into the cell while soaking the separators in electrolyte. The result of an incompletely soaked separator would cause only a fraction of the working electrode to undergo an electrochemical reaction, a situation that may lead to enormous experimental determination errors. Also, the simple fact of filling the cell with the right amount of electrolyte should not be overlooked. If there is not enough electrolyte, there could be a weak (high impedance) ionic contact, or rather no contact at all, between the electrolyte and the reference electrode leading to a non-functional test-cell.

While assembling the cells it is required to tighten all joints as firmly as possible and wrap them in Parafilm in order to further prevent electrolyte leaks or air contamination and therefore compromising the function of the battery.

3.2.3 Comparison of Errors in different Electrodes

In this work, various preparation methods were developed to assure a reproducibility of the results gained by testing of the accordingly built electrodes. These preparation methods consisted of the following procedures:

Procedure A: mixing of carbon (10 wt%), binder (10 wt%), silane (30 wt%), graphite (50 wt%) with N-methyl-2-pyrrolidone (NMP);

Procedure B: dissolving of the binder (4 wt%) and the silane (30 wt%) in NMP and subsequent mixing with carbon (4 wt%) and graphite (62 wt%);

Procedure C: ball-milling of the silanes (30 wt%) with graphite (62 wt%) and subsequent mixing with binder (4 wt%) dissolved in NMP and carbon (4 wt%);

Procedure D: ball-milling of all components (4 wt% carbon, 4 wt% binder, 30 wt% silane, 62 wt% graphite) including NMP

In order to compare multiple electrodes from different preparation methods, an additive calculation of the occurring errors was carried out. Therefore, considering Faraday´s law, the estimation of the experimental errors was done according to the expression below:

$$\frac{\Delta Q}{Q} = \frac{\Delta m}{m} + \frac{\Delta M}{M} + \frac{\Delta z}{z} + \frac{\Delta F}{F}$$

The values of maximum, minimum and average errors of the blank series were calculated using the experimental data of specific anodic capacity generated by Galvanostatic Cycling with potential limitation (GCPL). The calculations are based on the experimentally determined specific anodic capacities read at cycles 25 and 50; the corresponding results are displayed in Figure 3.

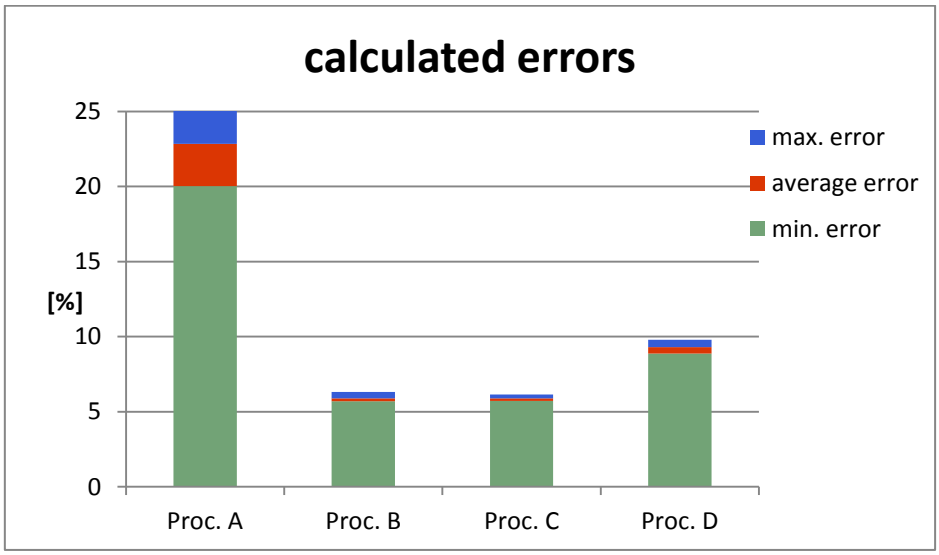

Figure 3: Calculated errors of the different blanks

Obviously, the samples containing graphite, binder and carbon only (further referred to as blanks) from Procedure A (simple mixing of ingredients) showed the largest distribution of capacities with an error of 25 %, followed by Procedure D (ball-milling all ingredients inclusive the solvent) that gives an error of approximately 10 %. On the other hand, procedures B (dissolving binder and silane in NMP before adding graphite) and C (Procedure B with additional ball-milling in dry state) both produced acceptably low errors of approximately 6 %. The remaining errors are caused by inaccuracy during weighing and possible weight loss during the assembly of the cells owing to scratches provoked by the used tweezers.

These results can be explained by the inhomogeneity of the samples resulting from insufficient solution of the binder. The binding polymer, if not dissolved properly, is known to form agglomerates and also to coat particles of graphite, hindering its electrochemical activity. This is the observed case for both the ball-milled and the un-milled samples including all ingredients at once. Additionally, samples created by Procedure A contain a larger amount of binding polymer (10 wt%) whereas all other procedures hold a mere 4 wt%.

3.3 Galvanostatic Cycling performed in Lithium-ion Battery Half-Cells

3.3.1 Samples containing perphenylated Silicon Rings

Galvanostatic Cycling with potential limitation (GCPL, cycling at constant current) was performed within the range of 0.02 to 1 V at a C-rate of C/2, always calculated with respect to the mass of graphite contained in each electrode. At least three electrodes of the respective series were tested in order to assure the reproducibility of any given effect and exclude malfunctions of the cells. Due to the different film-thickness and therefore assumed inhomogeneity of the film resulting from manual casting of the air-sensitive samples, only silicon containing samples could be tested in this manner. In order to compare the resulting capacity, an accordingly prepared blank, containing only graphite, conductive carbon and binder was used for reference in each procedure.

3.3.1.1 Series according to Procedure A

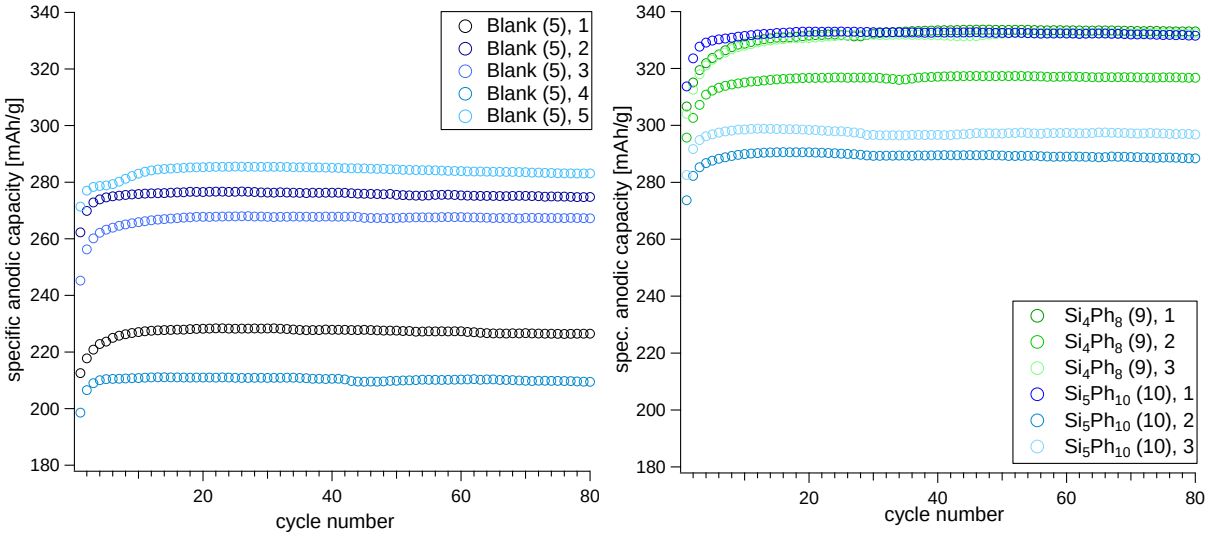

Figure 4: Galvanostatic Cycling of 5 (blank), 9 (Si_4Ph_8) and 10 (Si_5Ph_{10})

In Figure 4 the results of the GCPL for a blank as well as for $Si4Ph_8$ or Si_5Ph_{10} containing electrodes prepared according to Procedure A are displayed. The samples contained 30 wt% cyclosilanes, 50 wt% graphite and 10 wt% carbon and polyvinylidene difluoride (PVdF) binder each. Data achieved from Procedure A showed promising results at first, with both samples containing cyclosilanes exceeding the specific anodic capacity of their corresponding reference samples (blanks). Considering all of the results, samples including Si_4Ph_8 (**9**) exceeded the average capacity of the blanks (**5**, 253 mAh g^{-1}) by 29 % (327 mAh g^{-1}) and samples including Si_5Ph_{10} (**10**) by 21 % (306 mAh g^{-1}). Also, from the cycling data it can be seen that the capacity of the tested materials is stabilizing after 7-10 cycles. However, the dispersion of the experimental data between the datasets was very high, much higher than what a calculated error of 25 % would allow. Therefore these experiments were judged as irreproducible and the data was not considered for the final analysis. Additional electrodes from different series of the same composition were tested and these effects leading to higher capacity

could not be confirmed. This apparently higher capacity effects for samples containing silanes shown in Figure 4 (right) is likely to result from irregularities during the manufacturing of the electrodes or inaccurate weighing.

3.3.1.2 Series according to Procedure B

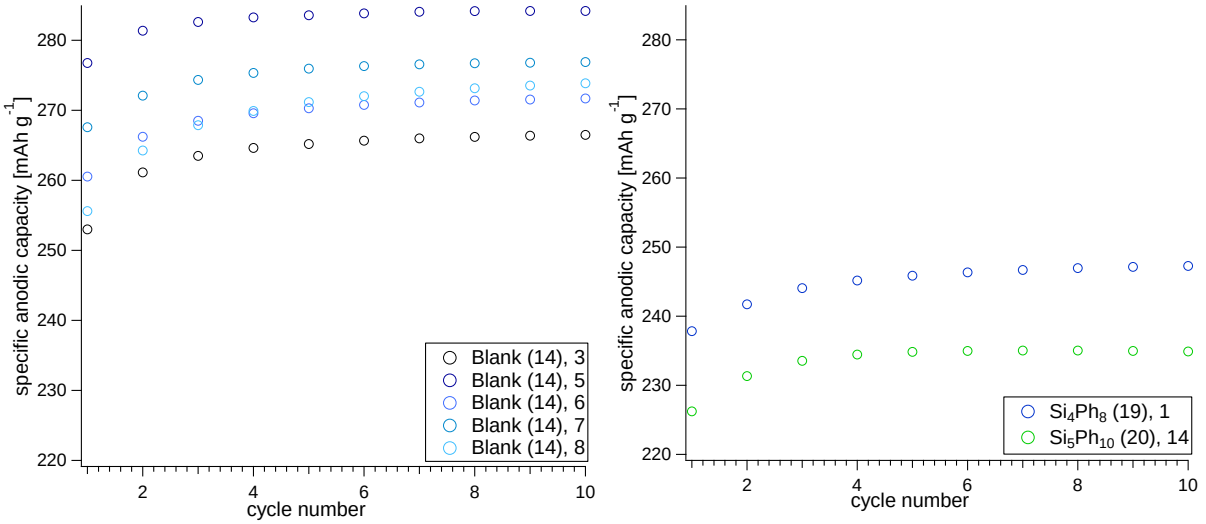

Figure 5: Galvanostatic Cycling of 14 (blank), 19 (Si_4Ph_8) and 20 (Si_5Ph_{10})

After several failed attempts with Procedure A, a change in composition and procedure was considered. Instead of the initial amount of 10 wt% of PVdF and carbon only 4 wt% were used for both. Additionally, all the polymer and cyclosilanes were dissolved in NMP before adding the remaining carbon and graphite. The initial amount of PVdF was chosen to assure an appropriate adhesion of the mixture on the copper surface. Electrodes prepared according to this procedure turned out to deliver a slightly brittle surface while keeping good adhesion to the metal. Experiments conducted with silane containing electrodes from Procedure B were interrupted after ten cycles due to a power-cut during the testing (Figure 5). Even though, the resulting data delivered a significantly lower dispersion (calculated error of 6 %) of the blanks (**14**) with an average specific anodic capacity of 275 mAh g^{-1}. In this case, sample **19** differed from **14** by 10 % (247 mAh g^{-1}) and from **20** by 15 % (235 mAh g^{-1}). Due to problems during the preparation of the electrodes such as crumbling of the coating material from the copper foil as well as short circuits after the assembly of the cells, no further optimization was carried out and a change in procedure was considered.

3.3.1.3 Series according to Procedure C

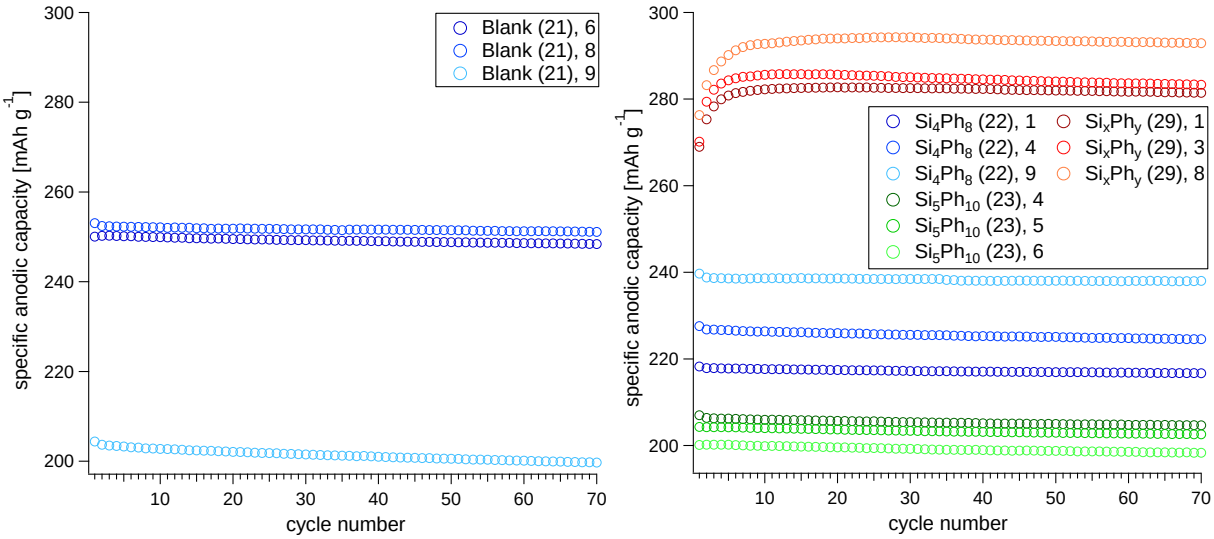

Figure 6: Galvanostatic Cycling of 21 (blank, right), 29 (Si_xPh_y), 22 (Si_4Ph_8) and 23 (Si_5Ph_{10})

Graphite and the cyclosilanes used for Procedure C were ball-milled in a planetary mill at 400 rpm. The resulting powder consisted of nano-particles which allowed an improvement of homogeneity in the slurry. Also, the change in structure of the graphite resulted in comparably lower specific capacity of the blank electrodes. PVdF was again dissolved in NMP before the addition of the remaining ingredients. Considering blank **21** (9) (Figure 6) as an anomalous point due to a problem during the assembly of the cell, the dispersion of the overall data was reduced to a minimum of 6 %. In comparison to the average specific anodic capacity of **21** (250 mAh g^{-1}), **22** offered a difference of 9 % (227 mAh g^{-1}) and **23** with 19 % (202 mAh g^{-1}) to its inferior. Therefore, an electrochemical contribution due to intercalation of the silanes into the graphite matrix is improbable. Rather, a formation of a layer coating the graphite, which causes a loss of capacity in comparison to sole graphite electrodes, is likely to occur.

However, data from the sample with the unknown composition Si_xPh_y (**29**) exceeds the blanks' capacity by 14 % (286 mAh g^{-1}) which is a significant amount above the error margin. This again reinforces the assumption of the existence of an additional component in the sample like a poly(diphenyl)silane which is contributing to the capacity by intercalation into the graphite layers, or by a direct and reversible reaction with lithium ions at the electrode. Further research on the exact structure of the sample and possible isolation of the contributing component will be conducted in the future.

3.3.1.4 Series according to Procedure D

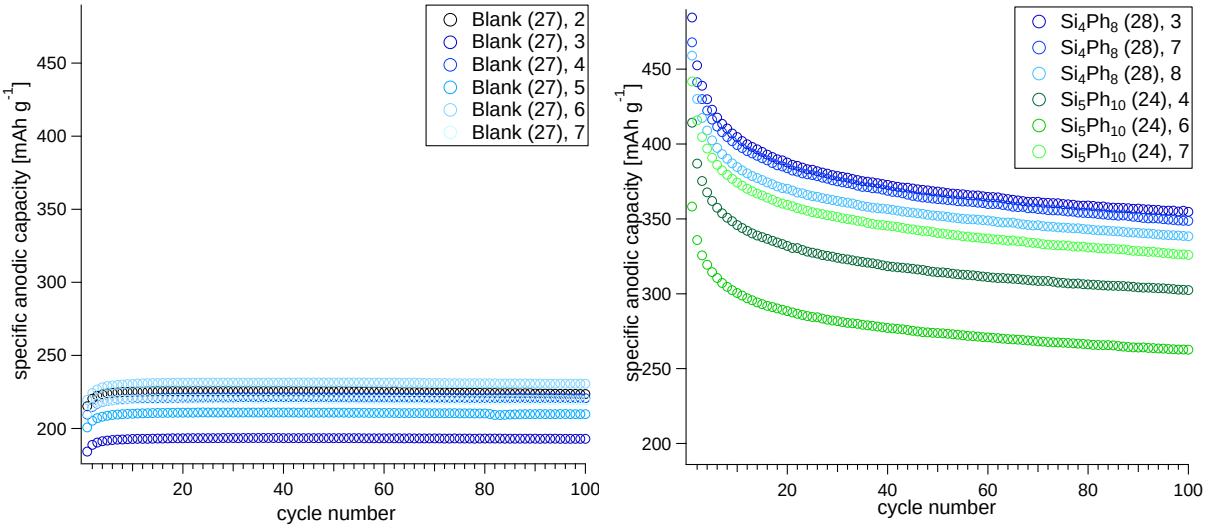

Figure 7: Galvanostatic Cycling of 27 (blank, right), 28 (Si_4Ph_8, pyrolysis) and 24 (Si_5Ph_{10}, pyrolysis)

In a further experiment, the pyrolysed cyclosilanes were mixed with the remaining ingredients (including the solvent; 46 wt% graphite and silane each, 4 wt% carbon and PVdF each) using the planetary mill at 400 rpm. The following tests resulted in a slightly higher but tolerable dispersion of the blanks capacities (approx. 9 %, Figure 7) which may be caused again by the PVdF, which might form small agglomerates of coated graphite due to incomplete dissolving and elevated temperature inside the beaker.

After an initially high specific anodic capacity of 470 mAh g^{-1} (**28**) and 405 mAh g^{-1} (**24**) respectively, both capacities sink continuously but the rate seems to stabilize towards the last cycles. A capacity degradation of approx. 27 % is being monitored over the measured cycles. Eventually, the resulting capacities for the pyrolysed samples exceed the blank (216 mAh g^{-1}) by 60 % (**28**, 347 mAh g^{-1}) and 37 % (**24**, 297 mAh g^{-1}). This result may be explained by an increase of the silicon content and decreased silicon to carbon ratio (Elementary Analysis). Also it indicates the existence of some nanostructured silicon in the electrode that adds up to the graphite´s electrochemical capacity. The continuous capacity degradation is possibly generated by the volume expansion of the silicon particles upon cycling, causing to fracture, or by the higher reactivity of the nanoparticles leading to a non-negligible, unwanted reaction with the electrolyte.

From data derived from these experiments, a specific capacity of the samples were determined to be 131 mAh g^{-1} for pyrolysed Si_4Ph_8 and 82 mAh g^{-1} for pyrolysed Si_5Ph_{10}.

3.4 Cyclic Voltammetry performed in Lithium-Ion Battery Half-Cells

The Cyclic Voltammetry (CV) investigation in lithium-ion battery half-cells was started with two consecutive scans at 1 mVs^{-1}, followed by a resting period of 12 h at open circuit voltage (OCV) afterwards. This was followed by Cyclic Voltammetry experiments at increasing scan rates. Two scans were done in succession for each of the following scan rates ranging from 0.05, 0.1, 0.2, 0.5, 1, 2 and 5 mVs^{-1}. All CV experiments were carried out within the potential range of 0 to 2 V. The data derived from measurements at 1 and 0.1 mVs^{-1} (first cycle of each scan rate) are being discussed below.

3.4.1 Perphenylated Cyclosilanes and Cyclogermanes

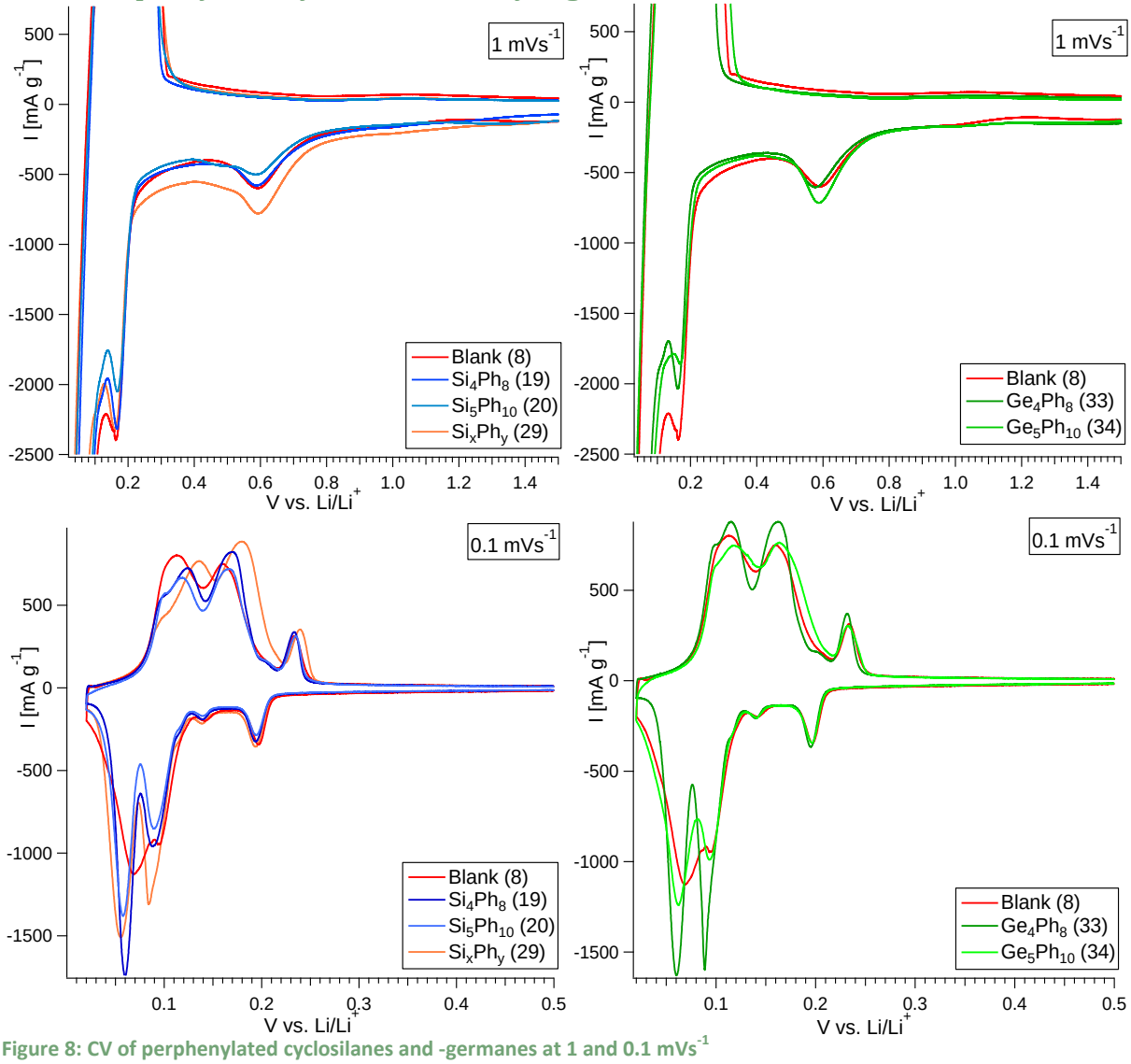

Figure 8: CV of perphenylated cyclosilanes and -germanes at 1 and 0.1 mVs^{-1}

Direct comparison of the perphenylated cyclosilanes and -germanes† with the respective graphite blank in CV measurements are shown in Figure 8. In the first cycles of both, cyclosilanes and -germanes at 1 mVs^{-1} a peak is visible at 0.6 V, which vanishes in later cycles. This might be caused by irreversible intercalation of lithium into the electrode during the first reduction process, or, more

†supplied by Prof. Scott Weinert, Oklahoma State University

likely, due to the formation of an SEI on the surface of the graphite by the reduction of electrolyte components. This reduction peak is not occurring in the following cycles. The influence of the cyclosilanes and -germanes is only hinted on by the minor increase of the current peak intensities at 0.2 V. This occurs for comparably high amounts for Si_xPh_y, confirming the results of the GCPL measurements.

Considering the curves at the rate of 0.1 mV s^{-1}, only reversible peaks appear after the first cycle. These peaks correspond to the formation of distinct LiC_x phases (x = 48, 32, 24, 12 and 6) commonly referred to as lithium insertion stages. The according delithiation steps are visible as peaks at 0.1, 0.15 and 0.22 V in the anodic scan. Since all of the tested materials show solely the same peaks as the graphite blank, a formation of amorphous silicon or germanium can be excluded.

A general trend may however be detected: both of the perphenylated four-membered ring systems show a higher current than their five-membered counterparts. In case of Ge_4Ph_8 the current is even exceeding the blank pointing towards some ring-opening. Regarding the curve of Si_xPh_y also a slight shifting of the peak towards higher potential is evident, which is caused by a component other than Si_4Ph_8 and Si_5Ph_{10} in the sample with a higher electrochemical activity. However, the mechanism leading to these capacity variation effects is not understood and further investigations are needed in order to establish and conclude on the reaction mechanism.

Nonetheless, further investigations of cyclogermanes have to be done.

3.4.2 Pyrolysed Samples

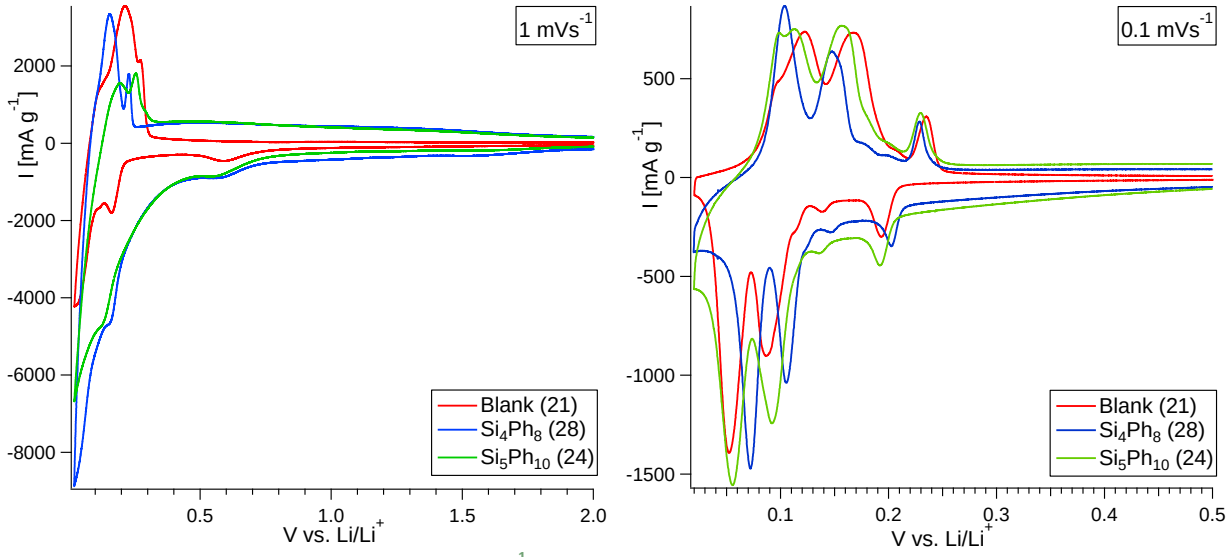

Figure 9: CV of pyrolysed products at 1 and 0.1 mVs^{-1}

Analogous to the untreated samples, all peaks (Figure 9) may be assigned to (de-)lithiation of the graphite in the electrodes. The pyrolysed products contribute to these peaks by distinctly shifting towards lower current and broadening of the reduction peaks (at 1 mVs^{-1}). This occurrence may be assigned to the increased amount of silicon, even though the formation of amorphous silicon may be excluded as well since all occurring peaks match the ones of graphite. The shift of the lithiation peaks towards higher potential (0.1 mVs^{-1}) suggests a higher electrochemical activity in comparison to graphite alone.

3.4.3 Samples including Tin

The tin-containing samples consisted of two different aryl substituted tin hydrides (aryl = mesityl, 1-naphthyl) (Scheme 5).[‡] These hydrides were used as prepared (a) (Scheme 6), as well as with the further addition of the base TMEDA to form a polymer *in-situ* in a solution of diethyl ether (Et_2O) (b). Additionally, a preformed naphthyltin-polymer derived from Et_2O (c) was tested.

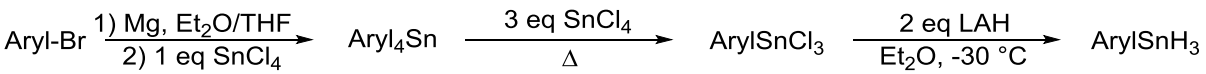

Scheme 5: Synthesis of $ArylSnH_3$ (Aryl = mesityl, 1-naphthyl)[36]

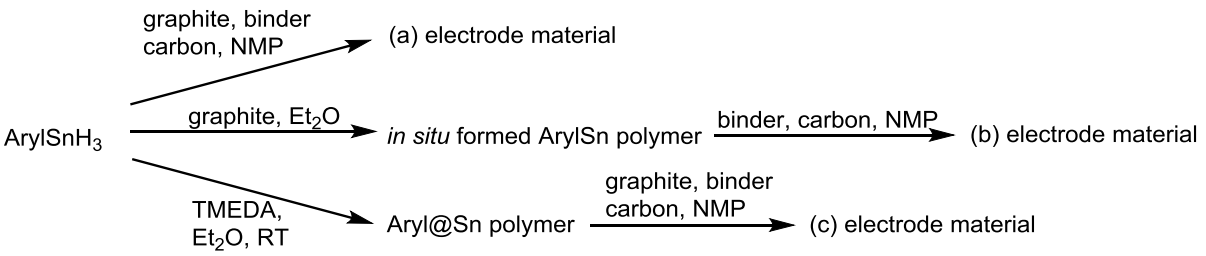

Scheme 6: Preparation of electrode materials from $ArylSnH_3$

[‡] supplied by Cathrin Zeppek, BSc MSc, Graz University of Technology

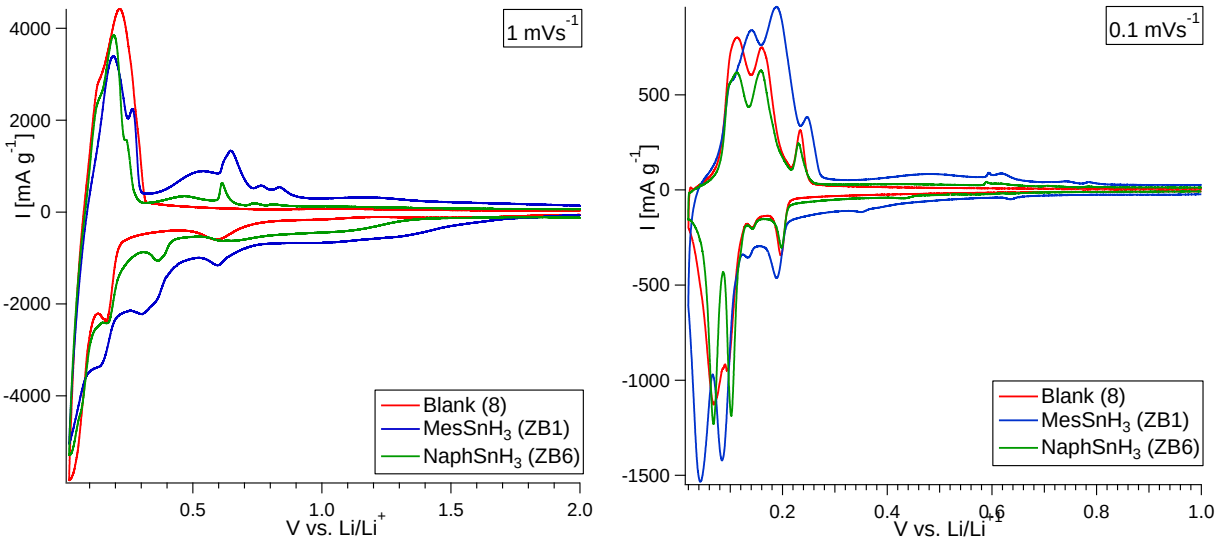

Figure 10: CV of $MesSnH_3$ and $NaphSnH_3$ (1 and 0.1 mVs^{-1})

Figure 10 shows a comparison of a graphite blank (**8**) and the differently substituted tin hydrides (**ZB1** (mesityl) and **ZB6** (naphthyl)) at rates of 0.1 and 1 mVs^{-1}. Both stannanes show an additional set of peaks not found in the blank, which broaden in following cycles but do not vanish. These broad cathodic peaks between 0.2 and 0.7 V can be ascribed to multistep electrochemical reduction reactions of tin with lithium to form various Li_xSn alloys.[40] Three anodic peaks (plus a shoulder at 0.5 V) between 0.5 and 0.8 V in the anodic scan may be assigned to extraction of lithium from the formed alloys. The remaining peaks that appear at lower potentials result from (de-)lithiation of the graphite matrix. These curves indicate a formation of nanostructured tin in the electrode, possibly in form of a core-shell particle.

Even though the stannanes show the same curves with differently distinctive peaks and shoulders, a higher electrochemical activity for **ZB1** is evident. Contrary to the expectation that additional aromatic groups would influence electrochemical activity of the electrode due to higher electron density, the mesityl group is more likely to intercalate into the graphite because of steric reasons and smaller size of the molecule. Additionally, the composition for the different samples varies slightly: for **ZB1** a content of 55.4 % graphite and 24.6 % $MesSnH_3$ was used, for **ZB6** graphite accounted to 55.1 % and $NaphSnH_3$ to 24.9 %. The influence of the composition for these samples is yet unknown, since only few tests were conducted.

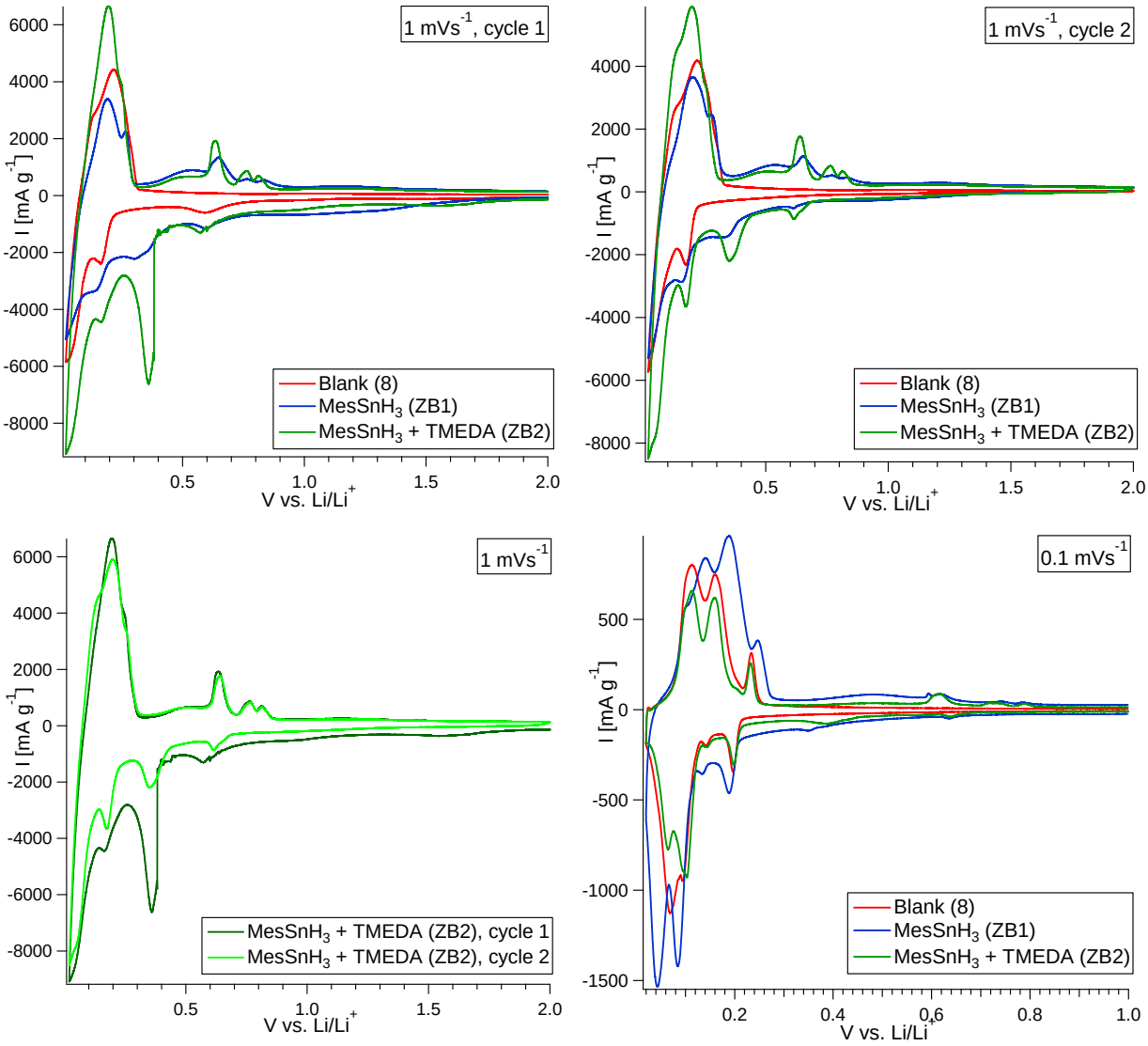

Figure 11: CV of $MesSnH_3$ with and without TMEDA (1 and 0.1 mVs^{-1})

In comparison of the samples including mesityl at 1 mVs^{-1}, a cathodic peak caused by **ZB2** (*in situ* formation of a polymer) at 0.4 V can be noticed (Figure 11, top left). This peak, diminishing in the following scans (Figure 11, bottom left), could be caused by three different occurrences. An irreversible capacity could be induced by lithium being trapped on specific sites such as the edges of the graphene layers, point defects or stacking faults. The stannane could possibly be involved in the formation of an SEI, an irreversible reaction, or this initial peak could also be caused by the formation of the polymer of hitherto unreacted stannane with TMEDA. The exact reaction is yet unknown. All emerging peaks of **ZB1** and **ZB2** are probably equivalent thus corresponding to the same process, although there are differences between them hinting about different reaction kinetics. It is evident, that an addition of TMEDA to the sample causes a higher electrochemical activity in comparison to graphite. However, this behaviour shows only in the first two scans (Figure 11, top). In further scans at different rates (e.g. at 0.1 mVs^{-1}), a convergence of the curve of **ZB2** to the blank curve is noticeable. Therefore it would be plausible, that any effect showing at the first two scans of **ZB2** is caused by completion of the polymerisation reaction.

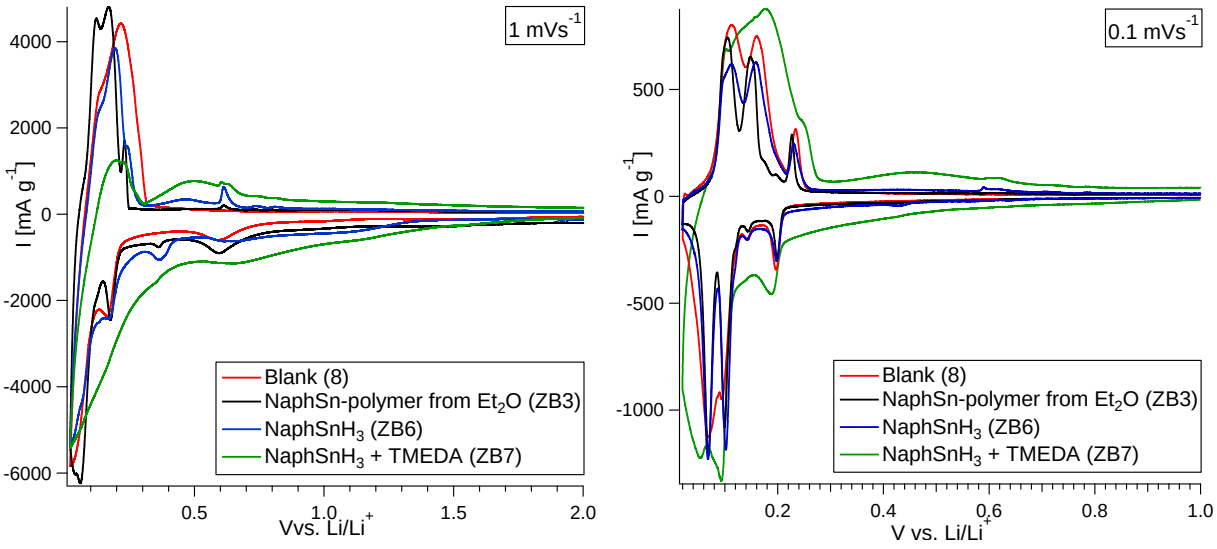

Figure 12: CV of Blank and NaphSn-compounds (1 and 0.1 mVs^{-1})

A comparison of the naphthyl-substituted stannanes shows similar results as for the mesityl-substituted ones. Remarkably in the first cycle at 1 mVs^{-1}, the pre-formed polymer **ZB3** shows a capacity exceeding the one for graphite alone. This effect already vanishes after the second scan and thereafter the electrode response is identical to the graphite blank sample. Similar to this behaviour, **ZB6** shows only the graphite response after a few cycles, but shows the most intense tin peaks in both, cathodic and anodic, scan. Interestingly, the polymer formed *in situ* (**ZB7**) shows rather the opposite: a higher electrochemical activity than the blanks' can be observed after several cycles (Figure 12, right). Also the characteristic tin-peaks appear to be broad and relatively shallow, a characteristic that would be consistent with the existence of an amorphous Sn-containing phase rather than having crystalline metallic tin.

By comparing the samples, different observations may be made. The pure tin hydride (**ZB6**) gives the most distinctive results for tin in graphite matrix[41] and a formation of nanostructured tin (possibly according to a core-shell model), able to intercalate into the graphite or covering it, is likely. The pre-formed and isolated aryl substituted tin-polymer gives less distinct but clearly observable tin-peaks. The disappearance of Sn-related peaks after several cycles suggests a cleavage of the polymer chain and further formation of nanostructured tin similar to the pure tin-hydride and out of electric contact. On the other hand, the curves recorded for *in situ* formation of the polymer suggest a partial polymerization reaction which is being completed during the electrochemical scan. As a consequence of the initially incomplete reaction, formation of smaller polymer fragments as well as unreacted tin-hydride is likely to interact with the graphite. Polymers that may be formed between the graphene planes are likely to strain the graphene layers or even exfoliate them. However, the resulting curves indicate that only a negligible part seems to be affected as the graphite continues to cycle well over many cycles.

3.5 Cyclic Voltammetry of Si_4Ph_8 and Si_5Ph_{10}

In this chapter, the most significant results of these measurements are discussed. Experiments performed at speed rates different from 10 mVs^{-1} had to be discarded due to less than optimal conditions leading to high levels of noise.

The procedure was set to start and finish at potentials close to the open circuit potential. In case of the blank solution, consisting of 0.1 M TBAP in THF, the open circuit potential was 0.2 V vs. ferrocene/ferrocenium hexafluorophosphate ($Fc/FcPF_6$)-reference. The term "semi-saturated" refers to the concentrations of the silanes corresponding to half the concentration of a saturated solution in THF.

3.5.1 Cyclic Voltammetry of THF and Si_4Ph_8

In Figure 13, the CV curves obtained for the blank and the Si_4Ph_8 containing solution are shown.

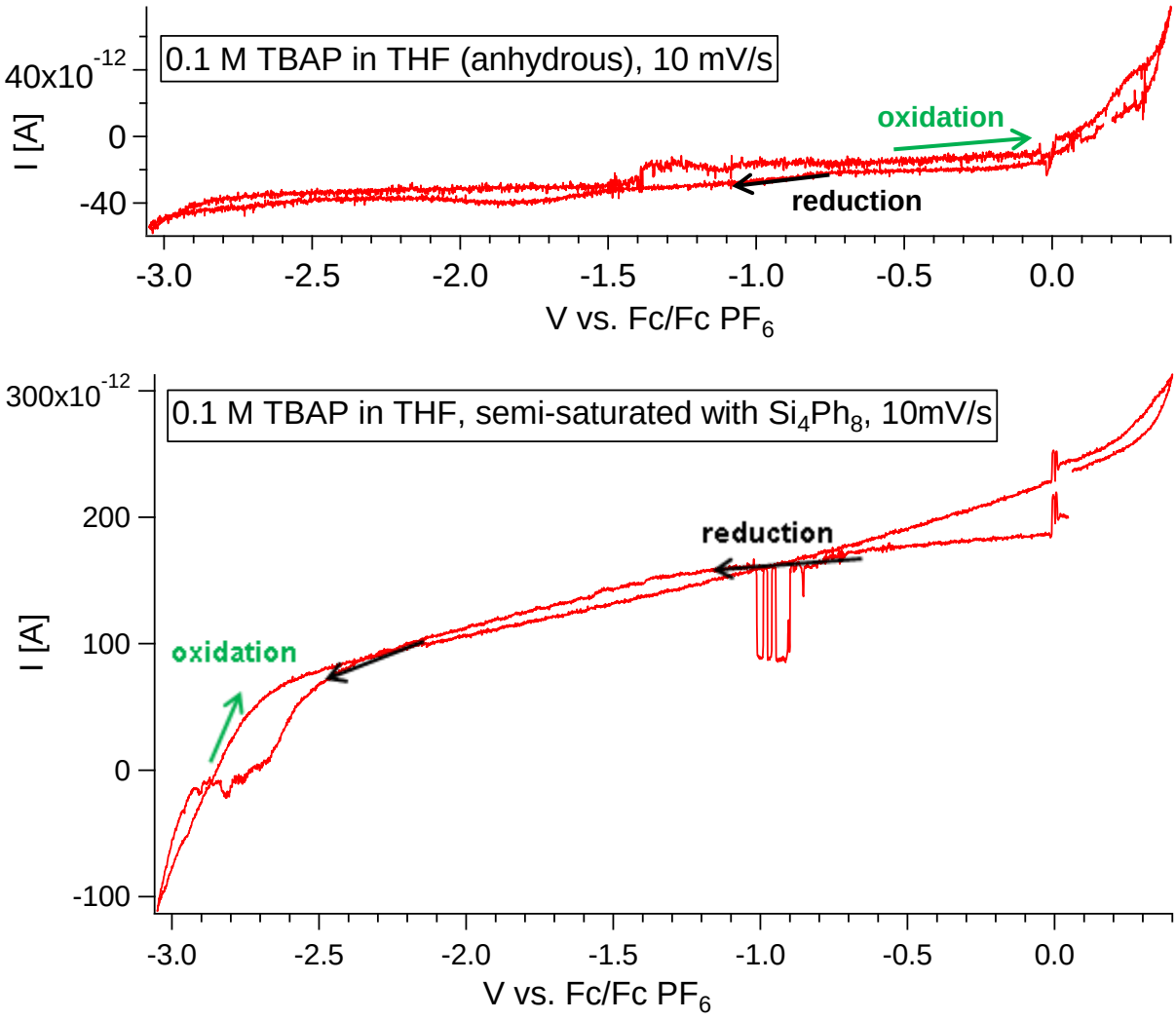

Figure 13: CV of THF (blank, top) and Si_4Ph_8 (bottom)

The blank's flat current ranges in approximately 130 pA and is therefore suitable for a background signal. Due to imperfections of the setup and very low currents, noise could not completely be prevented.

The peaks at approximately -1 V are artefacts and resulted from a change in the surrounding pressure inside the glove-box. From this data, the irreversibility of the reduction process can be observed, which starts at a potential of -2.6 V.

From the experimental data, different parameters such as electrode current density *j*, exchange current density j_0 and the charge transfer coefficient α_c may be determined using a Tafel-plot and the according Tafel equation, which is derived from the Butler-Volmer equation:

$$\eta = slope * \ln\left(\frac{j}{j_0}\right) \qquad \text{(Tafel equation)}$$

$$j = j_0 \left\{\exp\left[\frac{\alpha_a n F \eta}{RT}\right] - \exp\left[-\frac{\alpha_c n F \eta}{RT}\right]\right\} \qquad \text{(Butler-Volmer equation)}$$

j	electrode current density [A cm^{-2}]	F	Faraday constant (96485 [C mol^{-1}])
j_0	exchange current density [A cm^{-2}]	η	overpotential [V]
$\alpha_{a/c}$	cathodic/anodic charge transfer coefficient	R	univ. gas constant (8.3145 [J mol^{-1}K^{-1}])
n	number of electrons involved (electrode reaction)	T	temperature [K]

At large cathodic overpotentials, the anodic part of the Butler-Volmer equation can be neglected and hence the Tafel equation may be used instead. In case of the silanes studied, the cathodic part is of interest. Due to the fact that the exact mechanism is not yet known, it was assumed that one electron is involved in the electrode reaction.

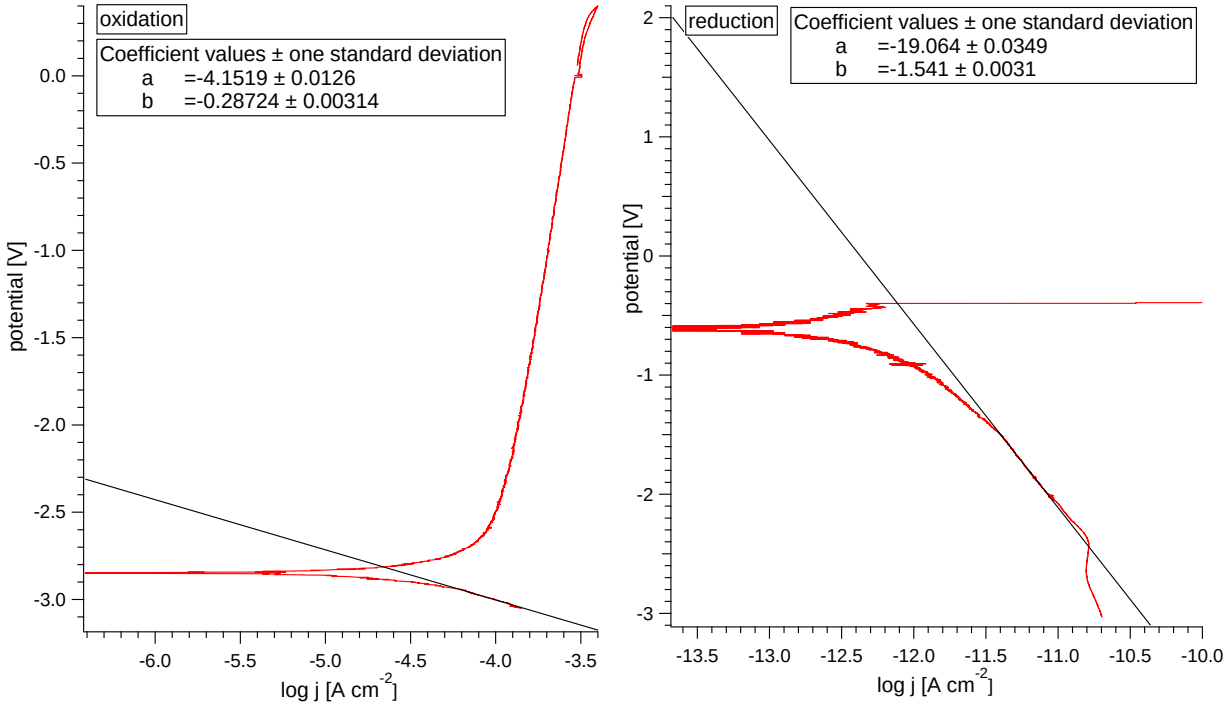

Figure 14: Tafel plots for Si_4Ph_8 (left) and Si_5Ph_{10} (right)

The Tafel plot for this experiment (Figure 14) showed two crosses through zero current instead of one which indicates a change in electrode surface and irreversible reaction. j_0 and α_c were calculated for Si_4Ph_8 using the oxidation peak and for Si_5Ph_{10} the reduction peak in cathodic direction. The electrode current density, j, was determined using the electrode surface of 7.85 * 10^{-7} cm^2, the exchange current density j_0 using the axis intercept *d* derived from the linear equation displayed. All equations used for the calculations are shown below.

$$\eta = slope * \log j_0 + slope \log j$$

$$slope = -\frac{2.303 * RT}{nF\alpha_c}$$

$$d = -slope * \log j_0$$

The exchange current density calculated for Si_4Ph_8 was j_0 = 2.89 * 10^{-5} A cm^{-2}. This indicates rather slower kinetics for this reaction. During the reduction a deposition of the material on the electrode is probable. As the silane itself is not charged, it is driven to the electrode not by electric charge but by diffusion.

The calculation of the cathodic charge transfer gave a value of α_c = 0.21. This also indicates a kinetically asymmetric reaction, with the equilibrium shifted to the educt side. Since the data shows many imperfections, the determination of the Tafel-slope might lead to some significant errors influencing the following Tafel-analysis.

3.5.2 Cyclic Voltammetry of Si_5Ph_{10}

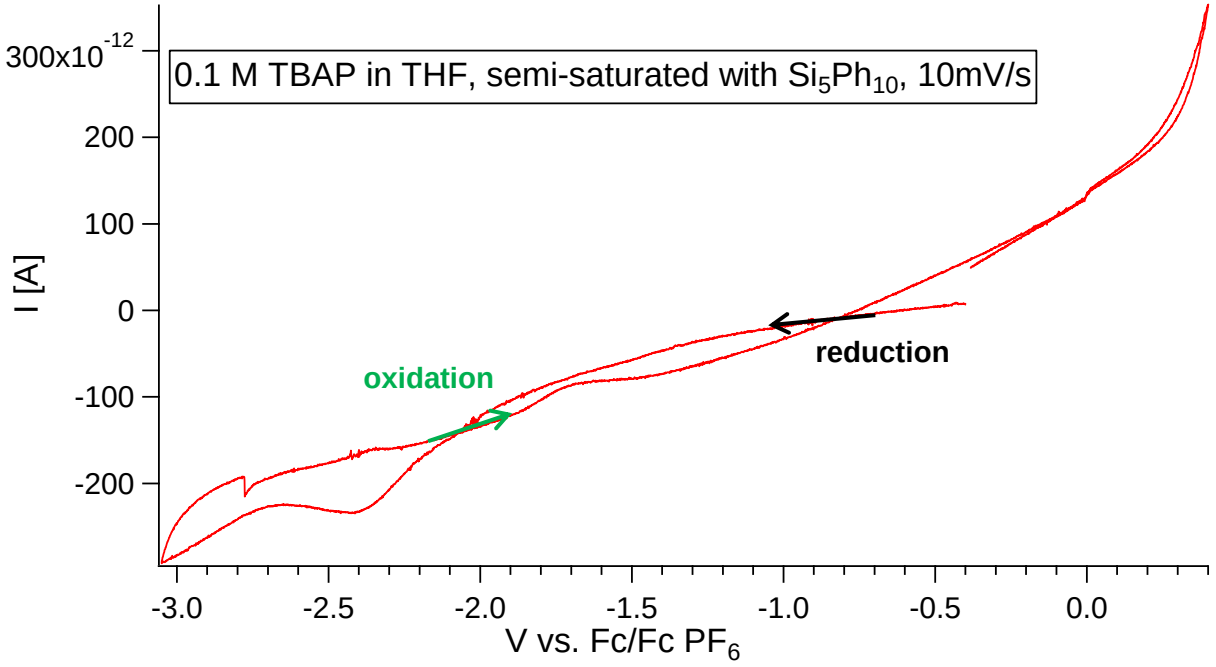

Figure 15: CV of Si_5Ph_{10} in THF/TBAP

The Cyclic Voltammetry of the cyclopentasilane (Figure 15) shows a partially reversible reaction identifiable by two shallow peaks at -2.4 (cathodic scan) and -1.6 V (anodic scan). The small peak at -2.8 V is an artefact due to contact imperfections.

The same as for the Si_4Ph_8, Tafel-plots (Figure 14) have been used for calculations of j_0 and α_c and gave values of $j_0 = 1.25 * 10^{-12}$ and $\alpha_c = 0.038$. In comparison to Si_4Ph_8, the exchange current density suggests very slow kinetics for its five-membered analogue. This could indicate a ring-opening reaction during the electrochemical reduction, which needs a higher activation energy than the one for four-membered cyclosilanes, due to lower ring-tension. Since the exact mechanism is yet unknown, more extensive investigation than conducted in the context of this work is necessary for detection of the same.

3.6 Synthesis

A major task in synthetic research was the attempt to generate cyclosilanes containing naphthyl moieties on the silicon ring. Their electrochemical properties should be compared with $(SiPh_2)_{4\text{-}5}$. However the synthesis of pernaphthylated cyclosilanes has not been successful so far.[42] Thus, it was focused on the synthesis of partly naphthyl substituted rings such as 1,2,3,4-tetraphenyl-1,2,3,4-tetranaphthyl-cyclotetrasilane ($[Naph(Ph)Si]_4$, **6**) or 1,2,3,4,5-pentaphenyl-1,2,3,4,5-pentanaphthyl-cyclopentasilane ($[Naph(Ph)Si]_5$, **7**).

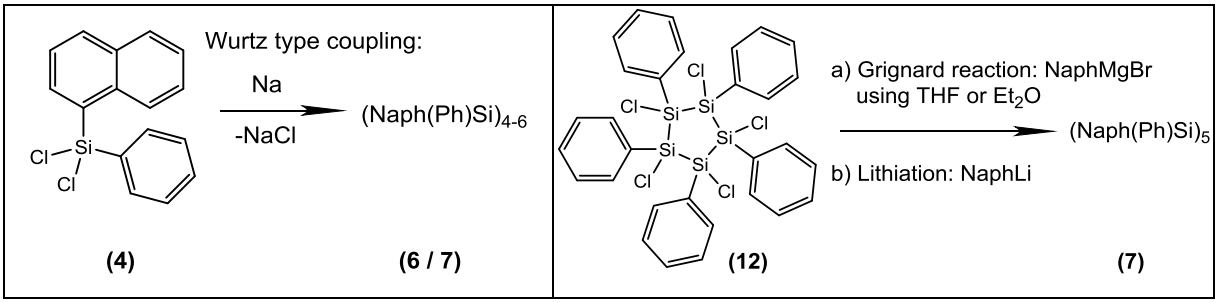

Scheme 7: Possible pathways leading to (Naph(Ph)Si)x

Preparation of such cycles (**6**, **7**) should be possible *via* different routes (Scheme 7). The first possibility is the Wurtz type coupling of dichloro-(1-naphthyl)(phenyl)silane (**4**). The second route is the conversion of a partially halogenated cyclosilane such as 1,2,3,4,5-pentachloro-1,2,3,4,5-pentaphenyl cyclopentasilane (**12**) with 1-naphthylmagnesiumbromide (Grignard approach) or 1-naphthyllithium (lithiation approach). Synthesis of the precursor (**4**) was tried *via* two routes: Grignard reaction and lithiation (Scheme 8 & 9, reactions **4 a-h**). Since both reaction pathways did not provide the desired product in acceptable yield and purity on first try, experiments were repeated using different parameters.

3.6.1 Synthesis of dichloro-(1-naphthyl)(phenyl)silane (4)

3.6.1.1 Grignard route

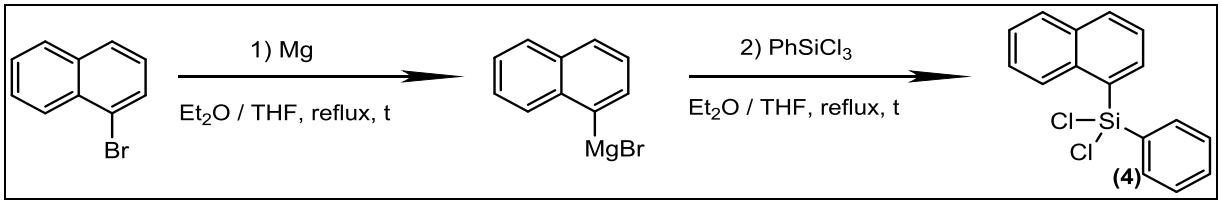

Scheme 8: Grignard route to $NaphPhSiCl_2$ (4)

The synthesis of $NaphPhSiCl_2$ was chosen according to Masuda and Stille[43], who used this compound in further reactions without purification. Here, the reaction parameters were changed several times in order to improve the procedure in terms of yield and purity of the product. All parameters used as well as observations made are listed in 4.3.2 Parameters for Grignard reactions.

Despite the fact that the experiment with the purest product (entry **4a**) resulted in 60 % $NaphPhSiCl_2$ (**4**) (according to GC-MS), two unknown side products emerged which were inseparable from the

product. Due to these side-products and the substituents on the silicon, a crystal structure could not be obtained. In fact, only few crystal structures of silicon dichlorides with two different aryl-substituents are known[44] which were obtained by lithiation.

3.6.1.2 Lithiation route

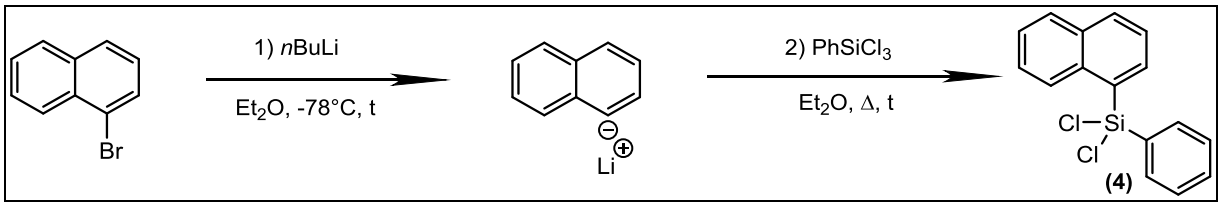

Scheme 9: Lithiation route to NaphPhSiCl$_2$ (4)

In several attempts, the educt ratio, stirring time for both reaction steps (Scheme 9) and the temperature at which the transfer was performed were varied. The exact parameters used are listed in 4.3.4 Parameters for lithiation reactions.

Entry **4h** successfully resulted in Naph(Ph)SiCl$_2$ (**4**) with a yield of 80 % (according to GC-MS). In this experiment, the reaction time was reduced to 1h for the lithiation and 1.5 h for the conversion of the lithiated species with trichlorophenylsilane (PhSiCl$_3$), respectively. Transfer temperature was lowered to -20 °C and also the lithium salt was removed immediately after completion of the reaction. The mixture was distilled under reduced pressure to remove the educts and give a white solid product. After distillation, only negligible amounts of side products were found. Less than 4 % could be detected by GC-MS. ^{29}Si-NMR showed only one peak at δ = 7.0 ppm, which is in accordance with the expected values for **4**. This expectation is based on a comparison of the NMR shifts of similar structures like dichloro-diphenylsilane Ph$_2$SiCl$_2$ (δ = 6.2 ppm)[45] and dichloro-dinaphthylsilane Naph$_2$SiCl$_2$ (δ = 7.3 ppm).[42] Integration of the peaks in the ^{1}H-NMR spectrum confirms the existence of compound **4**. An assignment of proton peaks of naphthyl and phenyl group was not possible due to overlapping signals not resolved.

4 Experimental

4.1 Methods

4.1.1 Cyclic Voltammetry

For the studies on reduction and oxidation processes occurring inside of a lithium-ion battery half-cell, Cyclic Voltammetry was conducted on a modular potentiostat/galvanostat/EIS (electrochemical impedance spectroscopy) VMP3 from *Bio-Logic Science instruments*. Data processing was carried out in the corresponding program *EC-Lab*, while plotting was done in *IGOR*.

4.1.2 Galvanostatic Cycling

Galvanostatic Cycling of batteries was performed using a *MACCOR* cell tester with a charge and discharge current corresponding to a C-rate of C/2, calculated from the battery capacity according to Faraday´s law (below). The C-rate is a measure of the rate at which a battery is charged or discharged in relation to its maximum capacity. In case of C/2 the necessary current is applied to or drained from the battery to charge or discharge it completely within two hours.

$$I = \frac{m \cdot F \cdot z}{t \cdot M}$$

I	current [A]	$z = \frac{1}{6}$	number of e^- exchanged / C atom
m	mass of electro-active material [g]	*M*	molar mass [g/mol]
F	Faraday´s constant [96485 C/mol]		

Considering the discharge reaction in the test cell (reduction process)

$$Li^+ + e^- + 6C_{(graphite)} = LiC_6$$

the following calculation was done for each electrode used:

$$I\ [A] = \frac{m\ [g] \cdot 96485\ [C/mol] \cdot \frac{1}{6}}{7200[s] \cdot 12[g/mol]}$$

Data processing was carried out in *MIMS* (the proprietary software for processing Maccor data files) followed by plotting in *IGOR*.

4.1.3 Nuclear Magnetic Resonance (NMR)

^{1}H (300.2 MHz), ^{13}C (75.5 MHz) and ^{29}Si (59.6 MHz) NMR spectra were recorded on a Mercury 300 MHz spectrometer from *Varian* at 25 °C. Chemical shifts are given in parts per million (ppm) relative to TMS (δ = 0 ppm). Coupling constants (J) are reported in Hertz (Hz). All NMR spectra were measured in C_6D_6. Reactions were monitored using a D_2O capillary as external lock signal.

4.1.4 Gas chromatography-Mass Spectrometry (GC-MS)

GC-MS spectra were recorded using an *Agilent Technologies* 7890A GC System coupled with a mass detector 5975C VL MSD (electron impact ionisation, 70 eV, carrier gas: helium). Spectra were given in abundance vs. time and abundance vs. mass-to-charge ratio respectively. Depending on the solvent, usually toluene or diethyl ether, different heating programs were used. In both cases a starting temperature of 40 °C was given and a final temperature of 280 °C was held for 10 minutes. The heating rate consisted of 12 °C/min for toluene and 18 °C/min for diethyl ether. Recording of the spectra started right away for diethyl ether and after 6 min for toluene.

4.1.5 Raman/Infrared (IR)-Spectroscopy

Comparative Raman spectra were recorded on a Raman station 400 F from *Perkin Elmer*, data processing was carried out using *Spekwin32*.

4.2 Experimental Settings and Apparatus

4.2.1 Swagelok® Cells

During this work, an electrochemical three electrode setup housed within a PFA-220-3 *Swagelok®* tube fitting was used to build Li-ion battery half-cells. This setup is airtight and fully suitable for electrochemical testing air- and moisture-sensitive materials such as the active materials used for Li-ion batteries. The steel parts were custom manufactured for this kind of cell (Figure 16). All test cells were assembled under protective atmosphere in an Ar-filled glove-box in which less than 1 ppm O_2 and H_2O vapours were present during cell assembly.

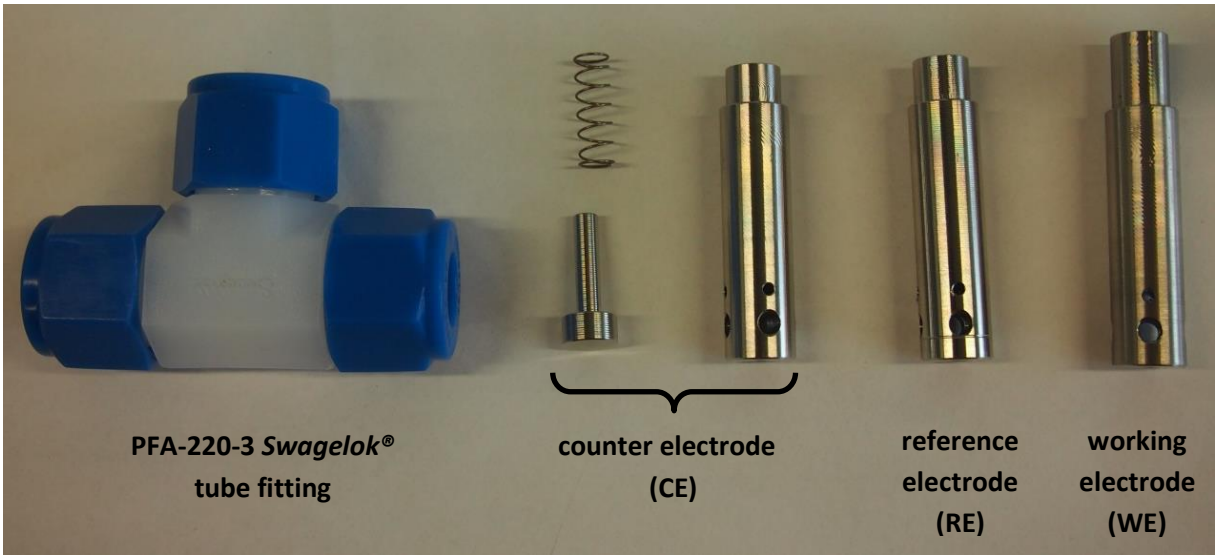

Figure 16: Swagelok® setup

For reference and counter electrodes, the corresponding steel parts were covered with a layer of lithium (lithium ribbon, 0.38 x 23 mm, *Sigma-Aldrich*, AT). The working/negative electrode, consisting of coated copper-foil (Preparation of Electrodes below), was contacted with the proper steel part. The assembly also contained two glass microfiber filter separators (Whatman, GF/B, Ø 1 cm, *GE*

Healthcare Life Sciences, AT) between the working and the counter electrode as well as one separator between the reference electrode and the rest of the cell. All separators were soaked in the LP30 electrolyte (1 M $LiPF_6$ in ethylene carbonate:dimethyl carbonate (EC:DMC) 1:1 vol., BASF, AT) before closing the cell tightly, avoiding the generation of gas-bubbles. In order to protect the cell´s steel parts from corrosion caused by an excess of electrolyte, especially at the RE, the device´s joints were eventually sealed with Parafilm.

4.2.2 Preparation of Electrodes

4.2.2.1 Chemicals and Materials

For the preparation of the required electrodes, a basic set of chemicals was indispensable: graphite (KS 6L, graphite, *Imerys Timcal C-NERGY*, CH), a binding polymer (*Kynar 761*, polyvinylidene difluoride, PVdF, *ARKEMA*, FR), a conductive additive (*Super C65*, conductive carbon black, *Imerys Timcal C-NERGY*, CH), a prospective active material to be mixed with graphite such as Si_4Ph_8, Si_5Ph_{10}, $MesSnH_3$, $NaphSnH_3$, Ge_4Ph_8 or Ge_5Ph_{10} and a solvent (N-methylpyrrolidone, NMP, *Sigma-Aldrich*, AT). A copper foil with rough surface (*Goodfellow Cambridge* Limited, 99.9 %, thickness 17.5 µm) was used as supporting metal and current collector.

4.2.2.2 Procedures

4.2.2.2.1 Procedure A: general approach

The first procedure consisted of pulverizing the active material using an agate mortar and simply mixing all components in a 10 ml polyethylene-vial (PE) including stirring at 600 rpm. After 12 to 24 h of stirring, the slurries were cast on copper-foil, using an *Erichsen Coatmaster 510* film applicator at a speed rate of 10 mm/s. The casting blade was set to give a film-thickness of 100 µm. Drying of the films in the oven at 60 °C for at least 12 h was followed by cutting several electrodes with a diameter of 1 cm. Subsequently, they were dried in a *Büchi Glass Oven* type *B-585*, at 60 °C for at least 12 h. The electrodes were weighed out on a *Mettler Toledo* XA105DU balance and dried again using the same conditions, before being transferred into a glove-box. Series that were prepared according to this pattern and their content are listed in Table 4.

Table 4: Contents of Series produced by Procedure A

series	type of electrode	graphite		silanes		binder		carbon		NMP
		[mg]	[%]	[mg]	[%]	[mg]	[%]	[mg]	[%]	[ml]
0	graphite blank	403.0	79.8	-	-	50.0	9.9	52.0	10.3	3.0
5	graphite blank	801.1	79.8	-	-	103.0	10.3	100.0	10.0	6.0
1A	Si_4Ph_8	352.0	70.0	50.0	9.9	50.0	9.9	51.0	10.1	3.0
2A	Si_4Ph_8	303.0	60.1	101.0	20.0	50.0	9.9	50.0	9.9	3.0
3A	Si_4Ph_8	250.1	49.8	150.0	29.9	51.0	10.2	51.0	10.2	3.0
9	Si_4Ph_8	250.4	49.9	150.1	29.9	50.2	10.0	51.0	10.2	3.0
1B	Si_5Ph_{10}	351.0	69.9	50.0	10.0	50.0	10.0	51.0	10.2	3.0
2B	Si_5Ph_{10}	302.0	60.0	101.0	20.1	50.0	9.9	50.0	9.9	3.0
3B	Si_5Ph_{10}	252.0	50.0	150.0	29.8	51.0	10.1	51.0	10.2	3.0
10	Si_5Ph_{10}	251.0	60.0	150.1	29.8	51.0	10.1	51.0	10.1	3.0

4.2.2.2.2 Procedure B: solution approach

In the second procedure, the binder was dissolved in 94 % of the NMP needed (usually 5.6 ml) and stirred for approximately 30 min. Carbon was added and the mixture stirred again for 30 min. After the addition of the remaining ingredients, the mixture was stirred for 24 h (in case of the blanks JB013 and JB014 also for 48 h) before casting on a copper foil with rough surface. Casting, drying and weighing of the samples were done analogous to Procedure A. Series that were made according to Procedure B and their content are listed in Table 5.

Table 5: Contents of Series produced by Procedure B

series	type of electrode	graphite		silanes		binder		carbon		NMP
		[mg]	[%]	[mg]	[%]	[mg]	[%]	[mg]	[%]	[ml]
13	graphite blank	800.0	79.7	-	-	104.0	10.4	100.0	10.0	6.0
14	graphite blank	921.0	92.0	-	-	40.0	4.0	40.0	4.0	6.0
19	Si_4Ph_8	620.4	62.0	300.1	30.0	40.0	4.0	40.0	4.0	6.0
20	Si_5Ph_{10}	620.4	62.0	300.2	30.0	40.1	4.0	40.0	4.0	6.0

4.2.2.2.3 Procedure C: ball milling (dry) approach

In this procedure, the pulverisation of the investigative material, of the graphite and components mixing were done using a *Fritsch Pulverisette* planetary micro mill with grinding beakers and grinding balls made of tungsten-carbide. A cycle of 10 min milling at 400 rpm and 5 min rest was repeated four times in order to avoid overheating of the samples placed within the beakers. The milled materials were then collected and used analogous to Procedure B, i.e. solvent added, mixed and cast on copper foil. Series that were prepared according to Procedure C and their content are listed in Table 6.

Table 6: Contents of Series produced by Procedure C

series	type of electrode	graphite [mg]	graphite [%]	silanes [mg]	silanes [%]	binder [mg]	binder [%]	carbon [mg]	carbon [%]	NMP [ml]
21	graphite blank	920.1	92.0	-	-	40.2	4.0	40.1	4.0	6.0
22	Si_4Ph_8	620.1	62.0	300.0	30.0	40.2	4.0	40.3	4.0	6.0
23	Si_5Ph_{10}	620.0	62.0	300.1	30.0	40.2	4.0	40.1	4.0	6.0
29	Si_xPh_y	875.8	62.0	423.8	30.0	56.5	4.0	56.6	4.0	6.0

4.2.2.2.4 Procedure D: ball milling (wet) approach

In Procedure D, all components of the slurries, including the solvent, were milled in the *Fritsch Pulverisette* planetary micro mill. This procedure was used for the preparation of electrodes containing the product of pyrolysis of Si_4Ph_8 and Si_5Ph_{10} only. The silanes were thermochemically decomposed at 700 °C under low argon-flow during 1 h, using a horizontal *Carbolite* GHA 12/600 glass-oven. Since these products are likely to adsorb oxygen in larger quantities, the samples were kept under inert atmosphere and the grinding bowls were loaded in a glove-box. The milling program was slightly altered for these samples to 1 h milling at 400 rpm without repetition. The milled slurries were then collected in 10 ml PE-vials and stirred again for 12 h at 600 rpm. Casting, drying and weighing occurred analogically to Procedure A. Series that were prepared according to Procedure D and their content are listed in Table 7.

Table 7: Contents of Series produced by Procedure D

series	type of electrode	graphite [mg]	graphite [%]	silanes [mg]	silanes [%]	binder [mg]	binder [%]	carbon [mg]	carbon [%]	NMP [ml]
27	graphite blank	1003.0	92.0	-	-	43.4	4.0	44.3	4.0	6.6
28	Si_4Ph_8, pyrolysed	650.9	46.0	650.0	46.0	56.7	4.0	56.5	4.0	6.6
24	Si_5Ph_{10}, pyrolysed	502.0	45.8	506.0	46.2	44.2	4.0	43.6	4.0	6.6

4.2.2.2.5 Procedure E: Stannanes and Germanes, air-sensitive materials approach

The electrode preparation for the air-sensitive stannanes and germanes was carried out entirely in a glove-box. The active-materials were combined with graphite in diethyl ether (anhydrous) and stirred for 30 min. For ZB002 and ZB007 where a tin polymer would be generated *in situ* 0.5 ml of TMEDA was added to this mixture. The solvent was evaporated under reduced pressure and the remaining binder, carbon and degassed NMP were added.

Casting of the film was carried out manually. The copper-foil was attached to an aluminium-plate in order to keep it in place. The casted films were dried overnight at 60 °C in a *Büchi Glass Oven* type *B-585* using an additional cooling-trap, which was removed after approximately 3 h. Also the cutting and weighing steps took place inside the glove box. Series that were prepared according to Procedure E and their content are listed in Table 8.

Table 8: Contents of Series produced by Procedure E

series	type of electrode	graphite [mg]	[%]	silanes [mg]	[%]	binder [mg]	[%]	carbon [mg]	[%]	NMP [ml]
8	graphite blank	803.0	79.8	-	-	103.0	10.2	100.0	9.9	6.0
ZB1	$MesSnH_3$	400.0	55.4	178.0	24.6	72.3	10.0	72.3	10.0	4.0
ZB2	$MesSnH_3$+TMEDA	400.0	55.7	173.0	24.1	72.3	10.1	72.3	10.1	4.0
ZB6	$NaphSnH_3$	441.0	55.1	200.0	25.0	80.0	10.0	80.0	10.0	4.0
ZB7	$NaphSnH_3$+TMEDA	440.0	45.8	328.0	34.2	96.1	10.0	96.2	10.0	4.0
33	Ge_4Ph_8	310.1	62.0	149.9	30.0	20.0	4.0	20.0	4.0	3.0
34	Ge_5Ph_{10}	310.1	62.0	150.0	30.0	20.0	4.0	20.0	4.0	3.0

4.2.3 Cyclic Voltammetry of Si_4Ph_8 and Si_5Ph_{10}

4.2.3.1 Chemicals

In Cyclic Voltammetry measurements, most chemicals were used as received from commercial sources or in-house production without further purification. The supporting electrolyte salt tetra-*n*-butylammonium perchlorate (TBAP, electrochemical grade, *Sigma-Aldrich*, AT) was purified by using multi-solvent recrystallization with analytical grade acetone and diethyl ether corresponding to Baron.[46] The commercially available tetrahydrofuran (THF, *VWR*, AT) was filtered through a drying-column-system (PureSolv MD3, *Innovative technologies, inc*.) and distilled over lithium aluminium hydride (LAH, *Sigma-Aldrich*, AT). Subsequently it was stored under nitrogen over activated molecular sieve to give a total water content of 23.5 ppm, controlled by Karl Fisher titration (conducted on a *TitroLine* KF trace).

4.2.3.2 Setup

A glass-cell with five joints (Figure 17) was used for all measurements. This setup was placed inside of an argon flooded glove-box, surrounded by a faraday cage and connected to an AutoLab galvanostat/potentiostat from *Metrohm*. The electrodes consisted of the following parts:

Table 9: Electrode Setup for Cyclic Voltammetry

electrode	components
working electrode	platinum microelectrode (10 µm diameter)
reference electrode	a) Haber-Luggin-capillary plus glass-frit filled with 0.1 M TBAP in THF b) a conjoining glass-frit filled with 4 mM ferrocene/ferrocenium hexafluorophosphate in 0.1 M tetra-*n*-butylammonium hexafluoro-phosphate (TBAF) in THF immersed into the filled capillary c) a platinum-wire immersed into b)
counter electrode	platinum wire grid

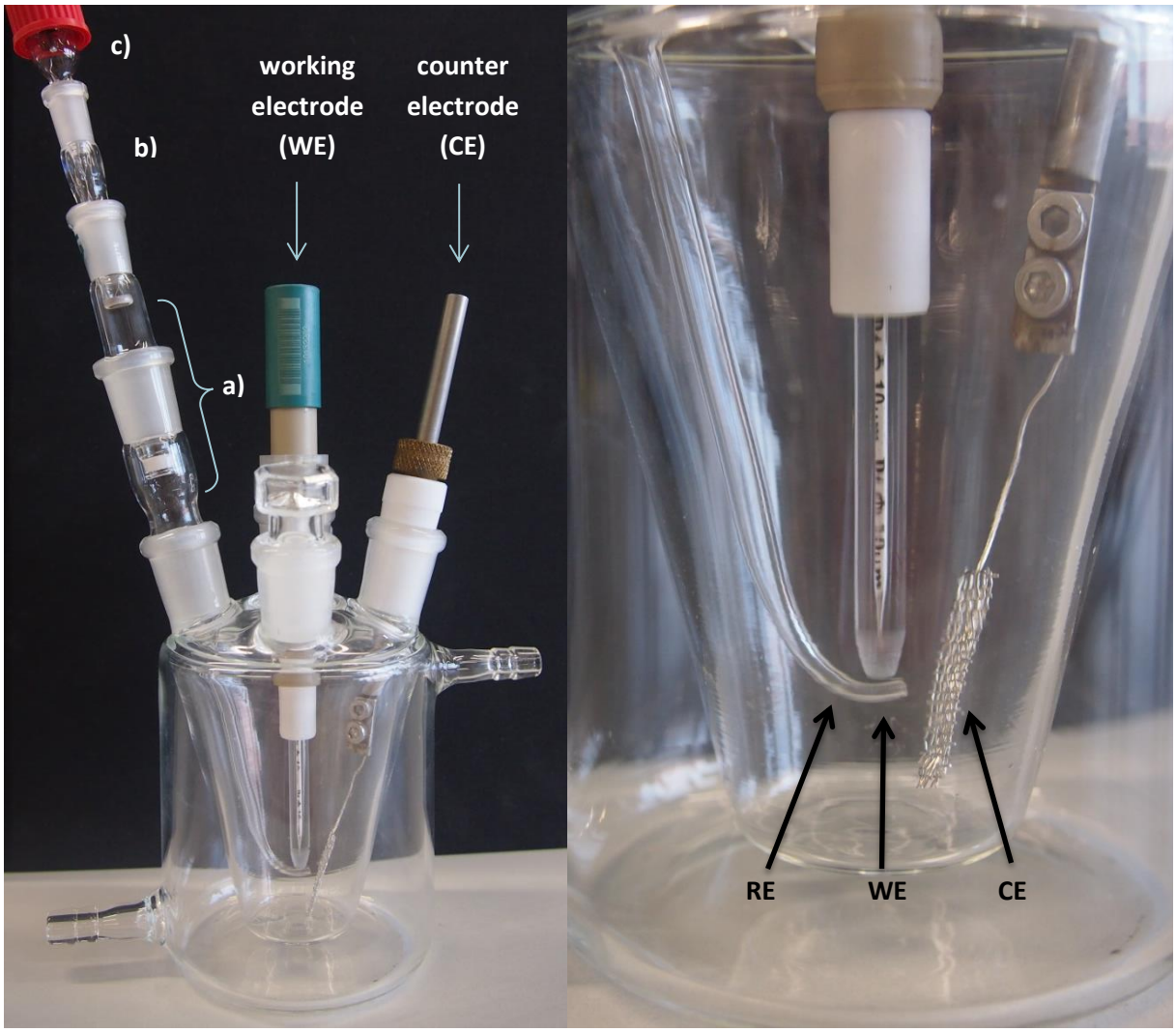

Figure 17: Setup for CV of Si_4Ph_8 and Si_5Ph_{10}

4.2.3.2.1 Procedure

The glassware needed was stored in an oven at 120 °C for 12 h, all non-glassy parts in an oven at 60 °C, before everything was transferred in a glove-box. The working electrode was polished with abrasive paper (silicon carbide paper, FEPA #4000, *Struers*) and subsequently rinsed with anhydrous THF. The cell was filled with the respective solutions to the level where every electrode was able to immerse into the electrolyte properly, usually about 20 ml. These electrolyte solutions consisted of 0.1 M TBAP in THF (blank), 0.1 M TBAP with 0.0014 M Si_4Ph_8 in THF or 0.1 M TBAP with 0.031 M Si_5Ph_{10} in THF. The concentrations of the silanes used correspond to half the concentration of a saturated solution in THF.

In a first step, the electrochemical window of THF was determined to lie between -3.05 V and 0.4 V vs. ferrocenium based reference (above) by cycling the blank solution (without perphenylated silicon rings) between different voltage limits (-3 V to 2 V, -5 V to 0.2 V and -3.5 V to 0.7 V) at a rate of 10 mVs^{-1}. The following measurements of all three electrolytes were carried out in the limits of this electrochemical window at increasing rates of 10 mVs^{-1}, 100 mVs^{-1}, 1 Vs^{-1} and 5 Vs^{-1}.

4.3 Preparation of dichloro-(1-naphthyl)(phenyl)silane (4)

Synthesis of dichloro-(1-naphthyl)(phenyl)silane (**4 a-h**: Naph(Ph)$SiCl_2$) was attempted *via* two routes: Grignard reaction and lithiation. All reactions were carried out using modified Schlenk technique. Here, an example for each procedure is specified below.

4.3.1 4 c *via* Grignard route

The reaction was carried out in a heat-dried three-necked flask equipped with reflux-cooler, gas tap, dropping funnel, bubbler and stirring bar under inert conditions. Magnesium (40 mmol, 0.97 g, 1 eq; Mg chips, *Sigma-Aldrich*, AT) was stirred vigorously in dry Et_2O and heated to start the exothermic reaction. 1-bromonaphthalene (40 mmol, 5.6 ml, 1 eq; 1-BrNaph, ρ = 1.48 g/ml, *Merck*, DE) was added drop-wise to maintain a constant reflux-rate. Upon completion of the addition, the brown solution was kept on reflux. The concentration of the Grignard reagent was determined by Gilman double titration[47] (0.5 ml Grignard reagent quenched with 20 ml deionized water (once with, once without 0.2 ml dry 1,2-dibromoethane in 3 ml diethyl ether), titrated against 0.1 M HCl with phenolphthalein as indicator). The Grignard reagent was transferred *via* cannula to an ethereal solution of phenyltrichlorosilane (40 mmol, 6.6 ml, 1 eq; $PhSiCl_3$, 97 %, ρ = 1.32 g/ml, VWR, AT) and heated to reflux to give a clear, brown solution.

The solvent was removed under reduced pressure and substituted with dry toluene to give a light yellow suspension. The colourless salt was removed *via* cannula and the solvent removed by distillation to give a brownish oil as product.

^{29}Si-NMR: δ = 6.9, - 13.5 ppm

4.3.2 Parameters for Grignard reactions

The reaction parameters have been changed for each synthesis attempt. They are listed in Table 10, containing the choice of solvent, reflux times for both reaction steps and additional work-up procedures. All experiments unfortunately resulted in inseparable product mixtures, thus another reaction route was chosen.

Table 10: Parameters used for Grignard reactions

entry	n [mmol]	solvent	reflux time [h] (1^{st}/2^{nd})		additional work-up
4a	500	THF	1	3	sublimation
4b	20	THF	2	3	none
4c	40	Et_2O	10	2	none
4d	75	THF	2	2	distillation

4.3.3 4 h *via* lithiation route

The reaction was carried out in a heat-dried two-necked flask equipped with gas tap and stirring bar. *n*-Butyllithium solution (44 mmol, 17.6 ml, 1.1 eq; in hexane, 2.5 M, *Sigma-Aldrich*, AT) was added drop-wise to an ethereal solution of 1-BrNaph cooled to -78 °C. The mixture instantly turned yellow

and discoloured after completion of the addition. The solution was stirred and allowed to warm up - 20 °C before transferring it *via* cannula to an ethereal solution of $PhSiCl_3$, cooled down to - 20 °C as well. The reaction was stirred and allowed to warm up to room temperature (RT). The colourless salt was removed using a filter cannula. The solvent was removed under reduced pressure to give a colourless solid as product.

^{1}H-NMR: δ = 8.55-8.44 (d, ^{3}J = 6.6 Hz, 1H (ar.)), 8.18 (m, 1H (ar.)), 8.02-7.82 (m, 2H (ar.)), 7.82-7.63 (m, 2H (ar.)), 7.62-7.12 (m, 6H (ar.)) ppm

^{29}Si-NMR: δ = 7.01 ppm

4.3.4 Parameters for lithiation reactions

All parameters used in the lithiation experiments are listed in Table 11, containing educt ratios, stirring time for both reaction steps, temperatures at which the reactants were transferred and the appearance of the resulting product.

Table 11: Parameters used for lithiation reactions

entry	1-BrNaph [mmol]	educt ratio (*n*BuLi : BrNaph : $PhSiCl_3$)			stirring time [h] (1^{st}/2^{nd})		transfer T [°C] (Li-species/$PhSiCl_3$)		product appearance
4e	20	1.1	1	1	2	10	0	0	brownish oil
4f	40	1.1	1	1	2	2	0	0	brownish oil
4g	40	1.1	1	1	3	10	-20	0	brownish oil
4h	40	1.1	1	2	1	1.5	-20	-20	colourless solid

5 Conclusion and Outlook

In this work, studies on the influence of four- and five-membered perphenyl cyclopolysilanes as well as of a sample of unknown composition Si_xPh_y on the capacity of graphite in Li-ion half-cells were performed. For this purpose, different preparation methods of the electrodes used were conducted. Testing of these electrodes was carried out using Galvanostatic Cycling and Cyclic Voltammetry protocols. Two general trends could be found:

a) the silane containing electrodes showed lower capacities than the comparably prepared graphite electrodes and

b) the capacities found for Si_4Ph_8 were slightly higher than for its five-membered analogue in all of the experiments performed. Additionally, an error estimation of each preparation method on the basis of the graphite (blank) electrodes was performed.

The Galvanostatic Cycling of the perphenylated cyclopolysilanes was carried out with electrodes from different preparation methods. The used electrodes differed in composition, particle size and treatment during the preparation. Taking the error estimations in account, the most reliable results were achieved by ball-milling the electrode materials (calculated error of 6 %). These electrodes contained 4 wt% binder, 4 wt% carbon, 30 wt% silanes and 68 wt% graphite. The resulting determined practical capacities were 250 mAh g^{-1} for graphite, 227 mAh g^{-1} for Si_4Ph_8 and 202 mAh g^{-1} for Si_5Ph_{10}. The average capacity of Si_xPh_y (286 mAh g^{-1}) exceeded the blank's by 14 %. As this result indicates the existence of a component other than the perphenylated cyclopolysilanes, an investigation on the exact structure of this compound should be conducted.

Exceptional results were found for electrode containing pyrolysed silanes, which elevated the average capacity significantly from 216 mAh g^{-1} (graphite blank) to 347 mAh g^{-1} (Si_4Ph_8, 60 % vs. blank) and 297 mAh g^{-1} (Si_5Ph_{10}, 37 % vs. blank).This may be explained by a ring opening during the pyrolysis at 700 °C, which resulted in shorter polymeric silicon structures. The pyrolysis might lead to higher capacity materials with experimentally found specific capacities of 131 mAh g^{-1} for pyrolysed Si_4Ph_8 and 82 mAh g^{-1} for pyrolysed Si_5Ph_{10}.

In order to determine the composition of the pyrolysed sample, powder diffraction X-ray measurements could be carried out. Furthermore, a series of the influence of different heat- and gas flow-rates on the composition of pyrolysed products and their corresponding effect in Li-ion batteries is a feasible goal.

Additionally to the perphenyl cyclopolysilanes, CV experiments in Li-ion half-cells were conducted with their corresponding germanium analogues. In both cases, no intercalation of elementary metal could be observed. This fact indicates a deposition of the compounds on the graphite surface inhibiting some of the electrochemical activity of the graphite rather than an insertion into the

graphene layers. The interactions between the cyclopolysilanes/ –germanes and graphite are yet unclear and further research is necessary to clarify it.

Cyclic voltammetry has also been performed with the tin trihydrides $MesSnH_3$ and $NaphSnH_3$ as well as with *in situ* and pre-formed polymers thereof. The stannanes all showed three distinctive oxidation peaks for elementary tin between 0.5 and 0.9 V vs. Li/Li^+. This indicated an electrochemical formation of smaller tin compounds, which are able to form alloys with lithium. An intercalation of the tin compounds into the graphene layers is also possible. A general trend towards the influence of the size of the aromatic substituents has not yet been found. Therefore, further investigations with different substituents such as anthracene should be conducted.
However, the degree of polymerization seems to have an influence on the cycling behaviour. A comparison between pre-formed and *in situ* formed tin polymers resulted in higher currents for the latter. This may be explained by the formation of smaller polymeric chains with hydride ending groups and a small amount of unreacted $ArylSnH_3$. These hydrides are easily electrochemically reduced to their radicals, which continue the polymerization within the graphite. The exact mechanism of the electrochemical reactions of the tin compounds in graphite electrodes and their long-time performance has yet to be clarified.

During this work dichloro-(1-naphthyl)(phenyl)silane ($NaphPhSiCl_2$) was successfully synthesized by lithiation reaction serving as starting compound for the preparation of aryl substituted cyclopolysilanes.

In further work, an improvement/optimization of the CV setup as well as the corresponding protocol is necessary in order to characterise the electrochemical properties of the perphenylated cyclopolysilanes. Possible additional characterisation methods include solid state NMR measurements of the compounds before and after cycling in Li-ion half-cells, as well as a possible electrochemical deposition of the compounds on electrode surfaces and scanning electron microscopy (SEM), transmission electron microscopy (TEM) or small angle X-ray scattering (SAXS) measurements thereof.

6 Appendix

6.1 Abbreviations

1-BrNaph	1-bromonaphthalene
CV	Cyclic Voltammetry
CVD/TVD	chemical/thermal vapour deposition
DMC	dimethyl carbonate
DME	dimethoxyethane
EC	ethylene carbonate
EIS	electrochemical impedance spectroscopy
ESR	electron spin resonance spectroscopy
Et_2O	diethyl ether
$Fc/FcPF_6$	ferrocene/ferrocenium hexafluorophosphate
GC-MS	gas chromatography mass spectroscopy
GCPL	Galvanostatic Cycling with potential limitation
Ge_4Ph_8	octaphenylcyclotetragermane
Ge_5Ph_{10}	decaphenylcyclopentagermane
IR	infrared spectroscopy
Li-GIC	lithium-graphite intercalation compound
$LiPF_6$	lithium hexafluorophosphate (electrolyte)
$MesSnH_3$	mesityltintrihydride
$NaphSnH_3$	naphthyltintrihydride
*n*BuLi	n-butyllithium
NMP	N-methyl-2-pyrrolidone
NMR	nuclear magnetic resonance spectroscopy
OCV	open circuit voltage
PE	polyethylene
$PhSiCl_3$	trichlorophenylsilane
PVdF	polyvinylidene difluoride
RT	room temperature
SAXS	small angle X-ray scattering
SEI	solid electrolyte interface
SiC	silicon carbide
(HR) SEM	(high resolution) scanning electron microscopy
Si_4Ph_8	octaphenylcyclotetrasilane
Si_5Ph_{10}	decaphenylcyclopentasilane
Si_6Ph_{12}	dodecaphenyl cyclohexasilane
TBAF	tetra-*n*-butylammonium hexafluoro-phosphate
TBAP	tetra-*n*-butylammonium perchlorate
TEM	transmission electron microscopy
THF	tetrahydrofuran
TMEDA	N,N,N´,N´-tetramethylethylenediamine

6.2 Index of Figures

6.3 Index of Schemes

6.4 Index of Tables

6.5 References

1 M.B. Armand, in *Materials for Advanced Batteries*, Plenum Press, New York, **1980**, 145.

2 J. Graetz, F. Wang, in *Nanomaterials for Lithium-Ion Batteries: Fundamentals and Applications*, Pan Stanford Publishing Pte. Ltd., **2014**, 69-94.

3 U. Kasavajjula, C. Wang, A.J. Appleby, *J. Power Sources*, **2007**, *163*(2), 1003-1039.

4 E. Hengge, M. Kira, H. Bock, *J. Organomet. Chem.*, **1979**, *164*, 277-280.

5 D. Linden, *Handbook of Batteries*, 2nd ed., McGraw-Hill, New York, **1995**, 2-4.

6 K. Nishio, N. Furukawa, in *Handbook of Battery Materials*, Wiley-VCH, Weinheim, **1999.**

7 M. Winter, J.O. Besenhard, in *Handbook of Battery Materials*, Wiley-VCH, Weinheim, **1999.**

8 K. Kinoshita, in *Handbook of Battery Materials*, Wiley-VCH, Weinheim, **1999.**

9 A. Hérold, *Bull. Soc. Chem. Fr.*, **1955**, *187*, 999.

10 X.Y. Song, K. Kinoshita, T.D. Tran, *J. Electrochem. Soc*,. **1996**, *143*, 6.

11 C. Hartwigsen, W. Witschel, E. Spohr, *Ber. Bunsenges. Phys. Chem.*, **1997**, *101*, 859.

12 J.R. Dahn, *Phys. Rev. B*, **1991**, *44/17* 9170.

13 V.V. Avdeev, A.P. Savchenkova, L.A. Monyakina, I.V. Nikol´skaya, A.V. Khostov, *J. Phys. Chem. Solids*, **1996**, *57*, 947-949.

14 N. Imanishi, Y. Takeda, O. Yamamoto, in *Lithium Ion Batteries* (Eds.: M. Wakihara, O. Yamamoto), Kodansha/Wiley-VCH, Tokyo/Weinheim, **1998**, 5.

15 M. Winter, J.O. Besenhard, in *Handbook of Battery Materials S2*, Wiley-VCH, Weinheim, **2011**, 469.

16 H. Shi, J, Barker, M.A. Saidi, R. Koksbang, *J. Electrochem. Soc.*, **1996**, *143*, 3466.

17 M. Winter, J.O. Besenhard, M.E. Spahr, P. Novák, *Adv. Mater.*, **1998**, *10*, 725.

18 C.K. Chan, H. peng, G. liu, K. McIlwrath, X.F. Zhang, R.A. Huggins, Y. Cui, *Nat. Nanotechnol.*, **2008**, *3*, 31-35.

19 L. Baggetto, P.H.L. Notten, *J. Electrochem. Soc.*, **2009**, *156*, A169-A175.

20 H.X. Zhang, C. Feng, Y.C. Zhai, K.L. Jiang, Q.Q. Li, S.S. Fan, *Adv. Mater.*, **2009**, *21*, 2299-2304.

21 B. Veeraraghavan, A. Durairajan, B. Haran, B. Popov, R. Guidotti, *J. Electrochem. Soc.*, **2002**, *6*, A675-A681.

22 Y.S. Sung, K.T. Lee, S.M. Oh, *Electrochim. Acta*, **2007**, *52*, 7061-7067.

23 M.K. Datta, P.N. Kumta, *J. Power Sources*, **2007**, *165*, 145-149.

24 F.S. Kipping, J.E. Sands, *J. Chem. Soc.*, **1921**, *119*, 830-847.

25 A.W.P. Jarvie, H.J.S. Winkler, D.J. Peterson, H. Gilman, *J. Am. Chem. Soc.*, **1961**, *83*, 1921-1924.

26 H. Gilman, D.J. Peterson, A.W. Jarvie, H.J.S. Winkler, *Tetrahedron Letters*, **1960**, *23*, 5.

27 H. Gilman, G.L. Schwebke, *J. Am. Chem. Soc.*, **1963**, *85 (7)*, 1016.

28 E. Hengge, R. Janoschek, *Chem. Rev.*, **1995**, *95*, 1495-1526.

29 H. Gilman, G.L. Schwebke, *Advan. Organomet. Chem.*, **1964**, *1*, 89.

30 Y.P. Wan, D.H. O´Brien, F.J. Smentowski, *J. Amer. Chem. Soc*,. **1972**, *94*, 7680.

31 F. Shafiee, R. West, *Silicon, Germanium, Tin Lead Compd.*, **1986**, *9,* 1.

32 E. Hengge, H. Firgo, *J. Organomet. Chem.*, **1981**, *212*, 155-161.

33 G. Becker, H.-M. Hartmann, E. Hengge, F. Schrank, *Z. Anorg. Allg. Chem*,. **1989**, *572*, 63.

34 R.K. Ingham, S.D. Rosenberg, H. Gilman, *Chem. Rev.*, **1960**, *60*, 459.

35 M.-L. Lechner, M. Trummer, I. Bräunlich, P. Smith, W.R. Caseri, F. Uhlig, *Appl. Organomet. Chem.*, **2011**, *25*, 769.

36 C. Zeppek, *Master Thesis*, **2012**, *Graz University of Technology*.

37 C. Zeppek, *unpublished research*, **2012**; HR-SEM carried out by the FELMI institute, Graz.

38 H. Tanaka, H. Ogawa, H. Suga, S. Torii, *J. Org. Chem.*, **1996**, *61*, 9402-9408.

39 D. Kovar, *Dissertation*, **1978**, *Graz University of Technology.*

40 Y.S. Jung, K.T. Lee, J.H. Ryu, D. Im, S.M. Oh. *J. Electrochem. Soc.*, **2005**, *152*, A1452-A1457.

41 C. Wang, Y. Li, Y.-S. Chui, Q.H. Wu, X. Chen, W. Zhang, *Nanoscale*, **2013**, *5*, 10599.

42 J. Krainer, *Diploma Thesis*, **2014**, *Graz University of Technology.*

43 T. Masuda, J.K. Stille. *J. Am. Chem. Soc.*, **1978**,. *100.*

44 J. Belzner, U. Dehnert, H. Ihmels, M. Hübner, P. Müller, I. Usón, *Chem. Eur. J.*, **1998**, *4*, No.5, 852-863

45 F. Uhlig, H.C. Marsmann, *"Silicon Compounds: Silanes & Silicones" Gelest, Inc.,* Morrisville, PA, **2008**, *208-222.*

46 R. Baron, N.M. Kershaw, T.J. Donohoe, R.G. Compton, *J. Phys. Org. Chem.*, **2009**, *22*, 1136-1141.

47 H. Gilman, F.K. Cartledge, *J. Organomet. Chem.*, **1964**, *2 (6)*, 447-454.